Astron. Astrophys. 327, 699–720 (1997)

ASTRONOMY AND ASTROPHYSICS

Wind variability of B supergiants

III. Corotating spiral structures in the stellar wind of HD 64760

A.W. Fullerton[1], **D.L. Massa**[2,⋆], **R.K. Prinja**[3], **S.P. Owocki**[4], **and S.R. Cranmer**[4,5]

[1] Universitäts-Sternwarte München, Scheinerstraße 1, D-81679 München, Germany
[2] Hughes STX, 7701 Greenbelt Road, Greenbelt, MD 20770, USA
[3] Department of Physics & Astronomy, University College London, Gower Street, London WC1E 6BT, UK
[4] Bartol Research Institute, University of Delaware, Newark, DE 19716-4793, USA
[5] Smithsonian Astrophysical Observatory, 60 Garden Street, Mail Stop 50, Cambridge, MA 02138, USA

Received 17 March 1997 / Accepted 19 June 1997

Abstract. Fourier analysis of two spectroscopic time series obtained with the *IUE* observatory confirm that the ultraviolet stellar wind profiles of HD 64760 (B0.5 Ib) are periodically variable. The periodic component consists of modulations that extend over most of the P Cygni absorption trough, and can frequently be traced through the emission lobe. The modulations coexist with variations due to the propagation of discrete absorption components, but there does not seem to be a direct link between these two types of variability.

In a long time series obtained in 1995 January during the *IUE* MEGA Campaign, the modulations in the P Cygni profiles of the Si III, Si IV, C IV, and N V resonance lines were dominated by two sinusoidal variations with semi-amplitudes between ∼5-10% of the continuum flux and periods of 1.202 ± 0.004 and 2.44 ± 0.04 days. The weak emission-lobe variability was predominantly due to the 2.4-day modulation. In the absorption trough, the ratio of the amplitude of the 1.2-day modulation to the amplitude of the 2.4-day modulation increased systematically as a function of ionization potential. For both periods, the distribution of the phase constant with position in the absorption trough exhibited a maximum near -710 km s^{-1}, and decreased symmetrically toward larger and smaller velocities. There was a systematic decrease in the value of the maximum phase between Si IV and N V. Only the 2.4-day period was present in a shorter time series obtained in 1993 March, when its amplitude was nearly twice its 1995 value and it was more concentrated toward smaller velocities in the absorption trough. There is no clear evidence for phase bowing in the 1993 data.

Since the 2.4- and 1.2-day periods are approximately a half and a quarter of the estimated rotational period of HD 64760, respectively, we interpret the modulations in terms of 2 (1993) and 4 (1995) broad, corotating circumstellar structures that modulate the optical depth of the stellar wind. The bowed distribution of phase implies that the structures are azimuthally extended, probably spiral-shaped arms, and we develop a kinematic interpretation of the projected velocity associated with the phase turnover in terms of the degree of bending of the spirals. We derive a value for the exponent governing the radial expansion of the wind of $\beta \approx 1$, which is in good agreement with the canonical value for smooth, spherically symmetric winds and suggests that the spiral structures are long-lived perturbations through which material flows. The systematic phase lag associated with higher ions suggests that they are preferentially located along the inner, trailing edge of the spiral, as expected if the structures are formed by the collision of fast and slow winds originating from equally-spaced longitudinal sectors of the stellar surface. Although a photospheric process is implicated in the origin of these structures, it is not clear that magnetic fields or nonradial pulsations could readily account for the switch between 2- and 4-equally spaced surface patches that evidently occurred between 1993 and 1995.

Key words: stars: early-type – stars: mass-loss – stars: oscillations – stars: magnetic fields – stars: individual: HD 64760 (HR 3090)

1. Introduction

Time-series spectroscopy of the P Cygni profiles of UV resonance lines obtained with the International Ultraviolet Explorer (*IUE*) satellite observatory has provided abundant evidence that the stellar winds of hot stars are variable in time. The most widely studied fluctuations are the discrete absorption components (DACs), which are optical depth enhancements that accelerate through the absorption troughs of unsaturated P Cygni profiles from low to high velocity much more slowly than the mean outflow; see Prinja (1992), Howarth (1992), and Henrichs et al. (1994) for recent reviews of the phenomenology associated with DACs. The intervals associated with both the recurrence

Send offprint requests to: alex@usm.uni-muenchen.de

⋆ Guest Observer with the IUE satellite, operated jointly by NASA, ESA, and PPARC

Table 1. Fundamental stellar parameters of HD 64760

Parameter	Value	Reference
Spectral Type	B0.5 Ib	Hiltner et al. (1969)
V	4.24	Hoffleit & Jaschek (1982)
$(B-V)$	-0.15	Hoffleit & Jaschek (1982)
$v \sin i$ [km s^{-1}]	238	Hoffleit & Jaschek (1982)
v_∞ [km s^{-1}]	1500	Massa et al. (1995b)
log $L_\star$ / $L_\odot$	5.1	Humphreys & McElroy (1984)
$T_{\rm eff}$ [kK]	23.1	Humphreys & McElroy (1984)
$R_\star$ / $R_\odot$	22	Humphreys & McElroy (1984)
$M_\star$ / $M_\odot$	20	Schaller et al. (1992)
Γ_e	0.17	derived [a]
$v_{\rm crit}$ [km s^{-1}]	380	derived [b]

[a] $\Gamma_e = 2.618 \times 10^{-5} \left(L_\star/L_\odot\right) \left(M_\star/M_\odot\right)^{-1}$ for Pop. I

[b] $v_{\rm crit} = 437 \left(M_\star/M_\odot\,(1-\Gamma_e)\right)^{\frac{1}{2}} \left(R_\star/R_\odot\right)^{-\frac{1}{2}}$

and evolution of DACs tend to anticorrelate with the projected rotational velocity, $v \sin i$, of the underlying star (Prinja 1988; Henrichs et al. 1988), which suggests that rotation is somehow connected with this phenomenon.

The recent *IUE* "MEGA Campaign" (Massa et al. 1995a) was designed to explore the nature of this connection by monitoring the behaviour of DACs in three early-type stars continuously over several consecutive rotational cycles. HD 64760 (HR 3090; also known as J Puppis) was an ideal target for this purpose, for three reasons. First, it is an apparently single, visually and UV-bright, intrinsically luminous field star with an early spectral type (B0.5 Ib according to Hiltner et al. 1969). As emphasized by the previous papers in this series (i.e., Massa et al. 1995b, hereafter Paper I; Prinja et al. 1997, hereafter Paper II), the UV spectra of early B stars of intermediate luminosity are ideally suited to studies of wind variability, particularly because they contain resonance lines of many species that exhibit well formed but unsaturated P Cygni profiles. Second, previous time-series observations obtained over 6 days in 1993 March had already demonstrated that the stellar wind lines of HD 64760 are quite variable, as the result of DACs and other, less localized fluctuations (Paper I). Third, HD 64760 has very broad photospheric absorption lines, which imply that it is a rapid rotator and therefore that several rotation cycles could be followed during an observing run of 2-3 weeks duration.

In fact, the projected rotational velocity of HD 64760 is quite extraordinary. According to Slettebak et al. (1975), the width of the He I λ4471 line corresponds to $v \sin i \approx 220\,{\rm km\,s^{-1}}$, which they noted is "unusually large for a star of luminosity class Ib". HD 64760 has the second highest $v \sin i$ in a sample of 48 supergiants with spectral types between O9 and B3 taken from the Bright Star Catalogue (Hoffleit & Jaschek 1982). This sample is characterized by a mean (median) $v \sin i$ of 93 km s^{-1} (87 km s^{-1}) and standard deviation 50 km s^{-1}. Thus, the observed $v \sin i$ of HD 64760 is 2.9 standard deviations from the mean value observed for stars of similar spectral type. If rotation is the dominant source of its line broadening, then this extreme value implies not only that HD 64760 is an intrinsically rapidly rotating star, but also that the inclination of its rotational axis to our line of sight must be quite large; i.e., $i \approx 90°$. On the basis of the adopted parameters of HD 64760 listed in Table 1 (in which all symbols have their conventional meanings), and including a conservative estimate of the uncertainty in the radius of $\pm 10\%$, the best estimate of its projected rotation period is $P_{\rm rot} = (4.7 \pm 0.4) \sin i \approx 4.7 \pm 0.4$ days. This is still well above the period associated with the "critical rotation" velocity ($v_{\rm crit}$; see Table 1), which corresponds to $P_{\rm crit} \approx 2.9 \pm 0.4$ days and which sets a lower limit on the inclination of $\sim 39°$.

The *IUE* MEGA Campaign was conducted in 1995 January, some 22.5 months after the 1993 campaign on HD 64760, and provided nearly uninterrupted coverage of its wind activity over an unprecedented interval of $\sim$16 days (approximately 3.4 rotational cycles). Along with the usual DACs, a surprising new form of stellar wind variability was detected, which consists of periodic changes in the flux of the entire absorption trough every $\sim$1.2 days (Prinja et al. 1995). The period associated with these variations is approximately a quarter of the assumed rotation period of HD 64760, which suggests that they may be due to 4 structures that corotate or nearly corotate with the stellar surface.

As a result of these developments, HD 64760 has emerged as a key object for studying the origin and nature of variability in hot-star winds. In this paper, we examine the properties of the new, periodic variations by studying the distribution of their amplitude, frequency, and phase as a function of position in the P Cygni profiles of the UV resonance lines of Si III λ1206, Si IV $\lambda\lambda$1394, 1403, C IV $\lambda\lambda$1548, 1551, and N V $\lambda\lambda$1239, 1243. The salient features of the 1993 and 1995 time series and their processing are reviewed in Sect. 2, while the properties of the newly detected variations are compared with the behavior of DACs in Sect. 3. The Fourier technique used to assess the harmonic content of the variations is described in Sect. 4, and applied to the time series data from the MEGA Campaign and the 1993 campaign in Sect. 5 and 6, respectively. Owocki et al. (1995) have already shown that the distribution of the cosine parameters as a function of position in a line profile provides constraints on the geometry of the wind structures, and some inferences based on this interpretation are developed in Sect. 7. Sect. 8 provides further discussion of some details of the model we propose to explain the stellar wind of HD 64760, along with suggestions for further work.

2. Observations and data processing

The *IUE* spectra from both the 1993 and 1995 campaigns were obtained through the large aperture with the high-dispersion mode of the SWP camera, and are characterized by spectral resolution of $\sim$13,000 ($\sim$0.1 Å) over the wavelength interval between 1150 and 1950 Å. Although the exposure time was always 60 seconds, the quality of 4 of the spectra from the 1993 campaign is quite low due to intermittent centering problems associated with the deterioration of the FES (Paper I). These spectra were excluded from the present analysis. The time sampling

Table 2. Properties of the IUE time series data for HD 64760

SWP No. (Range)	UT dates	HJD − 2 449 000.0	No. spectra	ΔT [days]	$\Delta t_{\rm min}$ [days]	$\Delta\nu$ [d^{-1}]	$\nu_{\rm max}$ [d^{-1}]
47097 – 47261	1993 Mar. 6-11	51.7830 – 57.5943	52	5.8113	0.0810	0.17208	6.17284
53339 – 53781	1995 Jan. 13-29	730.7797 – 746.5458	148	15.7661	0.0634	0.06343	7.88644

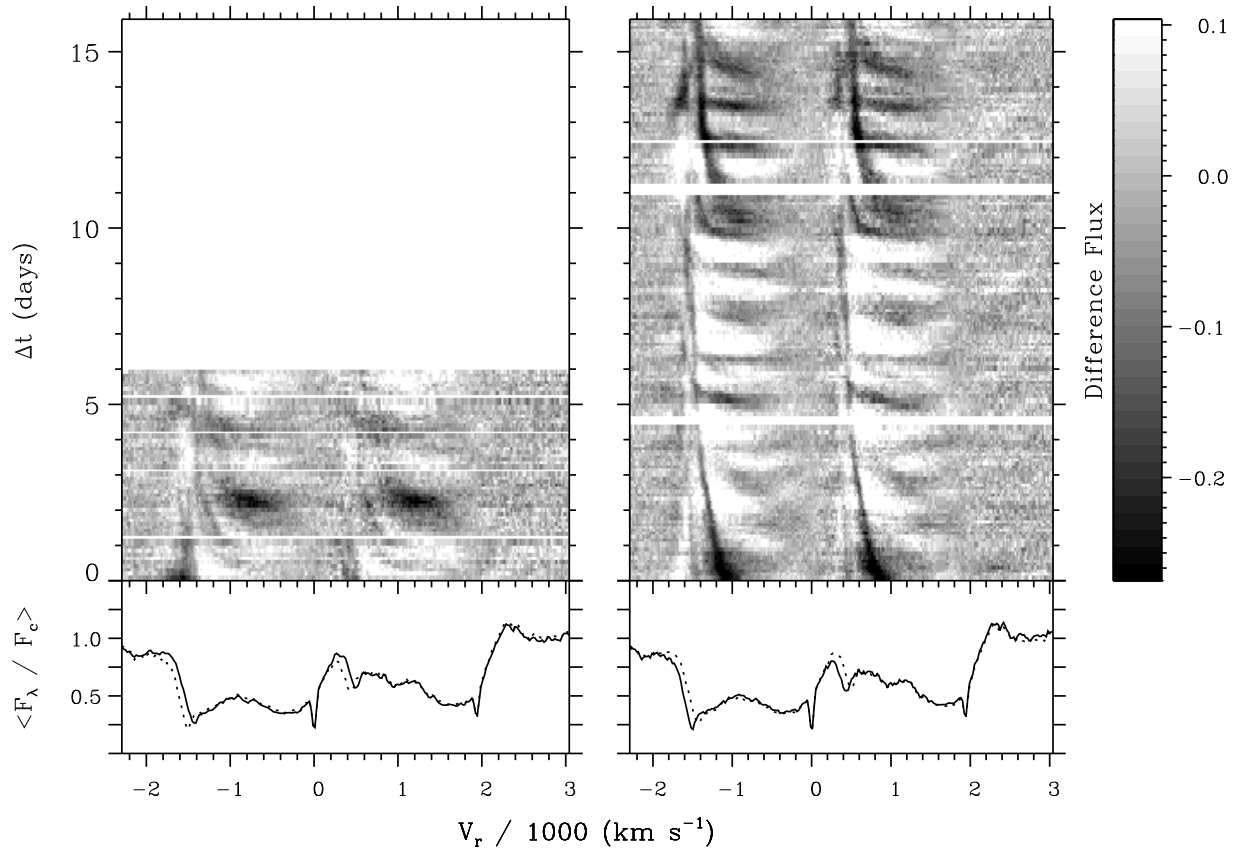

Fig. 1. Dynamic spectra of the Si IV doublet from 1993 (left) and 1995 (right; the MEGA Campaign). Darker shadings in the image denote places and times where a profile is deeper than its time-averaged value. Significant gaps in the time sampling have been left blank. The velocity scale for the mean profile in the lower panel refers to the blue component of the doublet. In the left panel, the solid and dashed lines represent the means of the 1993 and 1995 time series, respectively; vice versa in the right panel.

was approximately uniform during both campaigns, except for two large gaps of 6.5- and 8-hours duration in 1993 and 1995, respectively, that were imposed to accommodate a long-term AGN monitoring program. Table 2 summarizes the time sampling characteristics of the data, where successive columns list the range of SWP image numbers; the dates of the run in UT and heliocentric Julian date (HJD); the number of spectra obtained; the time in days between the middle of the first and last exposures of the run, ΔT; the minimum time between consecutive observations, $\Delta t_{\rm min}$, in days; and the corresponding frequency increment, $\Delta\nu$, and maximum frequency, $\nu_{\rm max}$, both in cycles per day. The latter two quantities are defined in Sect. 4.

The spectra were extracted and wavelength-calibrated in a uniform manner from the two-dimensional, photometrically linearized images by means of the IUEDR package (Giddings & Rees 1989). Spectra from each time series were normalized to a consistent pseudo-continuum by fitting splines to carefully selected regions in the vicinity of the spectral features of interest. The rectified spectra were rebinned to a constant wavelength step of 0.1 Å. Since each pixel in the rebinned spectra roughly corresponds to a spectral resolution element, they are approximately statistically independent of each other.

3. Description of the phenomenon

The components of the Si IV resonance doublet are the least blended of the important UV wind profiles, and consequently they provide the best illustration of the time-dependent be-

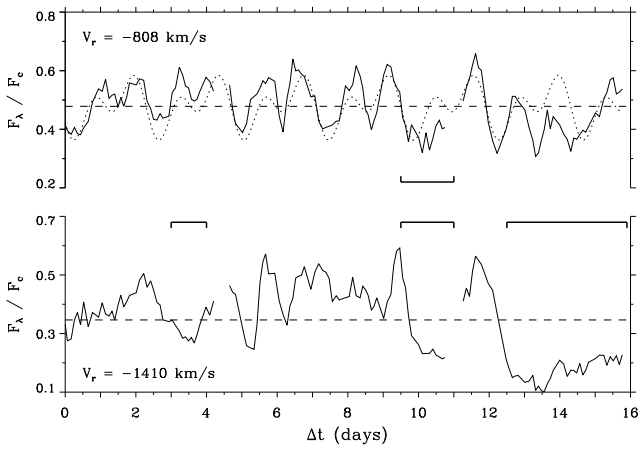

Fig. 2. The Si IV flux variations during the MEGA Campaign at positions in the absorption trough corresponding to line-of-sight velocities of -808 (upper) and -1410 km s^{-1} (lower). The mean flux level is indicated by a dashed line. A variation about this level composed of two sinusoids with periods of 1.2- and 2.4-days and semi-amplitudes of 6.5% and 6.2% of the continuum, respectively, is superimposed in the upper panel. Intervals when the flux is decreased due to the presence of a DAC are indicated by solid lines; see also Fig. 1. The variability at -808 km s^{-1} is mostly due to periodic modulations, while the variability closer to v_∞ is dominated by DACs.

haviour of the stellar wind of HD 64760. The spectroscopic time series of this line from 1993 and 1995 are presented in Fig. 1 in the form of grey-scale images ("dynamic spectra"). The contrast in these images has been enhanced by subtracting the respective mean spectrum from each member of the time series. Hence, regions and times of excess absorption with respect to the mean appear darker, while lighter shadings indicate intervals when the local flux was greater than its mean value. No interpolation or smoothing has been applied in either dimension. The mean spectrum from each time series is shown in the bottom panel of each frame. As noted by Prinja et al. (1995), they are quite similar, except near the high-velocity "blue edge" of the absorption trough.

The dynamic spectra in Fig. 1 show that the stellar wind of HD 64760 is extremely variable. Strong DACs are visible at large line-of-sight velocities near the beginning of both time series; they accelerate slowly to an asymptotic velocity of about -1500 km s^{-1} over the course of a few days, and become narrower as they move. In 1993, a second DAC appears at intermediate velocities near $\Delta t \approx 1$ day, and a third is visible at the end of the time series (see Paper I). In 1995, a second DAC appears near $\Delta t \approx 11$ days, and accelerates quite rapidly to a smaller asymptotic velocity than its predecessor; another DAC may also appear near $\Delta t \approx 9.5$ days. The difference spectra emphasize that the DACs always represent absorption excesses with respect to the mean value at a particular velocity.

However, the most noticeable variations in Fig. 1 are the series of alternating light and dark bands that run nearly horizontally across the absorption troughs of both members of the doublet, like rungs on a pair of ladders. These features are particularly prominent in the extended 1995 time series, where it is apparent from casual inspection that they repeat approximately periodically. Indeed, they are responsible for the 1.2-day periodicity detected by Prinja et al. (1995) in equivalent width measurements. In contrast to the DACs, these features occur over a broad range of positions in the absorption trough at every instant in time, and are characterized by intervals of lesser (darker) and greater (lighter) flux than the mean spectrum; i.e., the "rungs" are *modulations* about the mean flux level, not absorption excesses. Similar features are present in the 1993 time series, but are not as prominent since fewer cycles were covered during that run, both because the duration of that run was only $\sim$6 days and the period of the modulations was longer ($\sim$2.4 days) at that epoch (Sect. 6.1). Nevertheless, with hindsight it is clear that the peculiarly extended variations in the 1993 data that were labelled as the "main event" ($\Delta t \approx 1.6$ – 2.6 days), "the weakening period" ($\Delta t \approx 3.0$ – 3.7 days), and the "second major event" ($\Delta t \approx 3.8$ – 5.0 days) in Paper I should be interpreted as analogs of the modulations observed more prominently during the MEGA Campaign, and not as DACs.

The distinction between the DACs and the modulations is emphasized in Fig. 2, which shows the flux variations at two positions in the Si IV absorption trough that correspond to line-of-sight velocities of $V_r = -808$ and -1410 km s^{-1} (i.e., vertical cuts in Fig. 1 at these velocities). A wave characterized by two sinusoids with periods of 1.2 and 2.4 days with nearly equal semi-amplitudes (6.5% and 6.2% of the continuum, respectively) has been superimposed on the variations at -808 km s^{-1} in order to demonstrate that the new form of variability is indeed periodic, though the waveform is complicated. More importantly, these new variations consist of fluctuations above and below the mean level, i.e., the flux is continually modulated, not episodically enhanced. In contrast, the modulations are only weakly detectable at velocities closer to the terminal velocity, v_∞, where the variations are instead dominated by extended intervals of excess absorption due to the occasional passage of DACs.

Difference spectra for the Si III, Si IV, C IV, and N V resonance lines at the time of the MEGA Campaign are compared in Fig. 3, where the panels are arranged from left to right in order of increasing ionization potential. Analogous sequences of dynamic spectra for the 1993 campaign have been presented in Paper I, though in these images the modulations appear as absorption enhancements due to the bias introduced by renormalization with a maximum flux (minimum absorption) template spectrum. Although the different degrees of blending strongly influence the details of the appearance of the dynamic spectra, the behaviour of the modulations (and DACs) is qualitatively similar for the Si IV, C IV, and N V doublets. The modulations in the Si III resonance line are less distinctive, and occur over a longer time scale. Although these differences are partially due to the inferior quality of the data for this line (owing to the rapid decline in the sensitivity of the SWP camera blueward of $\sim$1230 Å), they also emphasize that the phenomenon responsible for the modulations manifests itself differently in lines of different ionization potential.

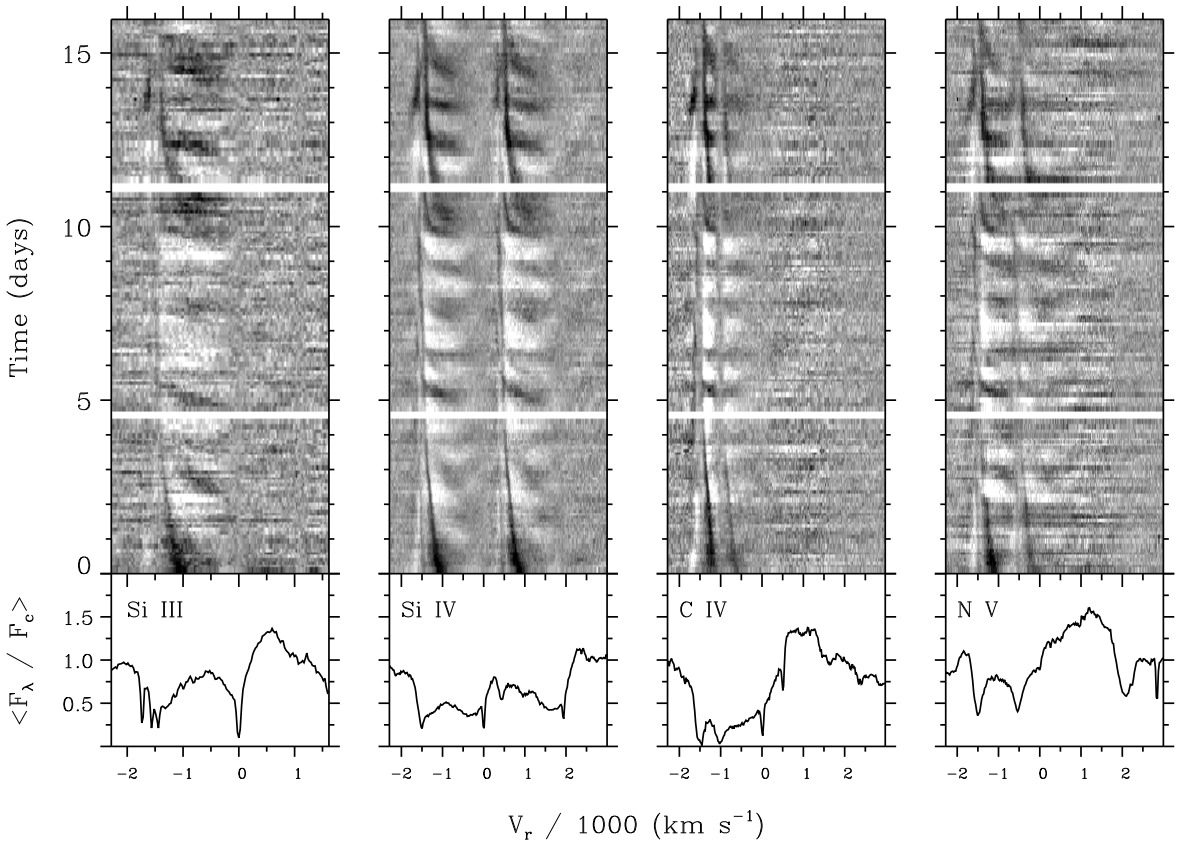

Fig. 3. Comparison of the dynamic spectra for the Si III, Si IV, C IV, and N V resonance lines observed during the MEGA Campaign. The grey scale is the same for all images, and corresponds to differences from the mean spectrum ranging from −30% (black) to +19% (white) of the continuum.

Several other interesting properties of the modulations in the 1995 data can be glimpsed in the dynamic spectra. The first and most important property is that the modulations tend to bend "upwards" in the direction of increasing time, so that a particular phase of the modulation occurs first at an intermediate velocity, and then reaches higher and lower velocities *simultaneously* at a later time. This "phase bowing" is especially evident in the dynamic spectra of Si IV and N V: the light contour with minimum near Δt = 2.0 days is a good example of phase bowing that can be traced across the entire width of the Si IV and N V profiles. The bowing is harder to see at low velocities in Si III and blending seriously compromises its visibility in C IV.

Second, although the modulations are most prominent in the absorption trough, Figs. 1 and 3 show that they can be often followed to positions that lie within the weak emission lobe of the red component of the line. These features appear as linear extensions towards increasing time of the modulations in the low-velocity part of the absorption trough. Once again, these modulations can be seen most clearly in Si IV and N V, where they can sometimes be traced to velocities approaching +500 km s^{-1} in the frame of the red component of the doublet.

Finally, the modulations sometimes extend beyond the asymptotic velocity of the DAC; see, e.g., the absorption excesses at Δt = 5.2 and 13.5 days in the dynamic spectra (Figs. 1, 3). When this happens, there is no obvious interaction with the DAC itself. Indeed, there does not appear to be any particularly clear relationship between the modulations and the occurrence or propagation of the DACs in either the 1993 or the 1995 time series.

3.1. Representation in terms of cross-correlation functions

Without interactive colour-table manipulation, some of the properties of the modulations described above are difficult to see in the dynamic spectra. Their visibility can be enhanced by computing the temporal correlation of the flux variations at successive positions through a P Cygni profile with respect to the flux variations at a fiducial position in the profile. Conceptually, this amounts to shifting a given flux vector $F_\lambda(t, \lambda)$ with respect to the fiducial flux vector $F_\lambda(t, \lambda_{\rm ref})$ by some amount of time, τ (the lag). For a given lag, the cross-correlation is the convolution of the two functions: in the case of periodic variations, it will be large if the lag is an integral multiple of the period (i.e., the time shift puts $F_\lambda(t + \tau, \lambda)$ in phase with the fiducial flux vector) and small if the lag is an integral half-multiple of the period. The cross-correlation function is less sensitive to noise than the original spectra because data from all the cycles sampled contribute to the correlation function at each lag, with the

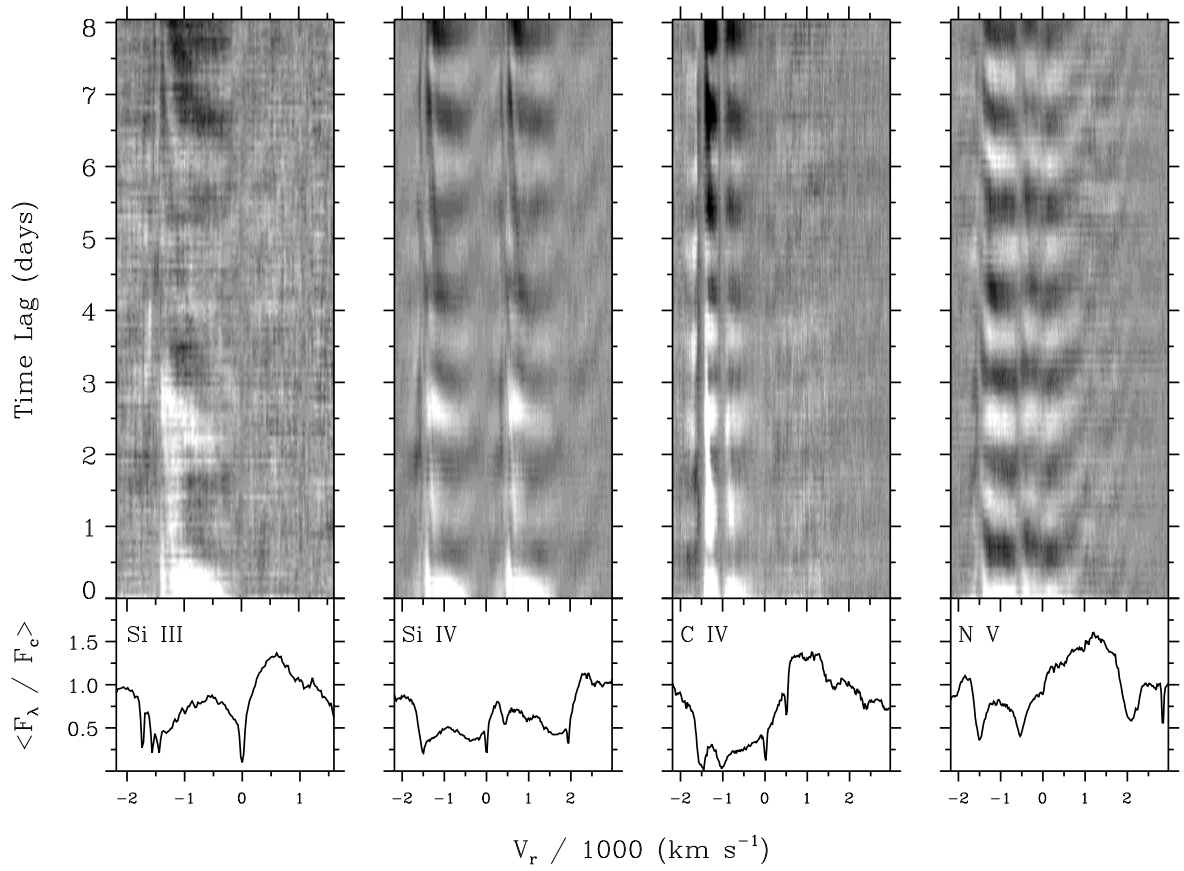

Fig. 4. Correlograms for the Si III, Si IV, C IV, and N V resonance lines during the MEGA Campaign. Light and dark shadings correspond to degrees of positive and negative correlation with the flux variations at -700 km s^{-1}, respectively. The intensity scale is the same for all images.

result that subtle features associated with each repetition of the modulation can be distinguished more easily.

We computed cross-correlation functions for the major wind lines observed during the MEGA Campaign by using the Fourier technique described by Scargle (1989) to circumvent the difficulties introduced by irregular time sampling. The flux variations at -700 km s^{-1} (in the frame of the blue component in the case of doublets) in each line were used as the fiducial vector in these calculations, the results of which were arranged in matrix format so that successive columns contain the cross-correlation function for adjacent spectral resolution elements. Fig. 4 presents these "correlograms" for the resonance lines of Si III, Si IV, C IV, and N V in an image format that is entirely analogous to the dynamic spectra of Fig. 3, except that the independent variable is the time lag rather than the time. The phenomenon of phase bowing is seen especially clearly in the correlograms for Si IV and N V; in the latter case, the two extremes of the bow are visible in different components of the doublet. The extension of the modulations to velocities blueward of the terminal velocity (-1500 km s^{-1}) is demonstrated very clearly in this representation of the time series, as are the modulations of the emission lobes.

4. Time series analysis

Since the dynamic spectra from the MEGA Campaign provided such clear evidence for periodic variability, we were encouraged to perform a more detailed time series analysis of the modulations. Our technique is based on the discrete Fourier transform (DFT), and is essentially identical to the procedure introduced by Gies & Kullavanijaya (1988) to study photospheric line profile variations. A one-dimensional DFT, $f(\nu_i)$, is computed from the flux variations $F_\lambda(t)$ at each spectral resolution element λ_j (or its corresponding line-of-sight velocity, $V_{r,j}$) in the time series. The frequency grid on which $f(\nu_i)$ is calculated, ν_i, is determined by the (unequal) sampling characteristics of the time series, and is defined by a maximum frequency, $\nu_{\rm max} = 1/(2\,\Delta t_{\rm min})$, and a frequency increment, $\Delta\nu = 1/\Delta T$. These quantities are given in Table 2 for the *IUE* time series of HD 64760. For practical reasons, it is desirable to oversample the frequency increment by a small factor: here, we used an oversampling factor of 4.

Since the variations discussed here are well sampled in time, their spectral window functions are not especially complicated. Nevertheless, we used the iterative CLEAN algorithm (Roberts et al. 1987) to deconvolve the features of the window function from the DFT. Our implementation of the DFT routine for un-

equally spaced data and the CLEAN algorithm consist of a suite of procedures in Interactive Data Language (IDL) that are based on the FORTRAN programs distributed by Roberts et al. (1987). We experimented with various combinations of the parameters that control the iterative removal of the window function (i.e., the "gain", which is the fraction of the window function that is removed per iteration, and the number of iterations) but did not find substantial differences between the resultant CLEANed Fourier transforms (CDFTs). All the CDFTs discussed in this paper have been CLEANed for 200 iterations with a gain of 0.2.

The ensemble of CDFT vectors for a range of wavelengths can be conveniently stored as a column in a complex, two-dimensional array, $f(\nu_i, \lambda_j) \equiv f_{ij}$. A single row in this array records the CDFT at temporal frequency ν_i for all wavelengths, while a single column contains the DFT at all temporal frequencies for position λ_j. Consequently, for each position λ_j in a spectral line, the semi-amplitude, $A(\nu_i, \lambda_j) \equiv A_{ij}$, and phase, $\phi(\nu_i, \lambda_j) \equiv \phi_{ij}$ associated with the sinusoid of frequency ν_i are given by

$$A_{ij} = 2\left((\mathrm{Re}\,\{f_{ij}\})^2 + (\mathrm{Im}\,\{f_{ij}\})^2\right)^{\frac{1}{2}} \quad (1)$$

and

$$\phi_{ij} = \arctan\left(\mathrm{Im}\,\{f_{ij}\} \,/\, \mathrm{Re}\,\{f_{ij}\}\right) \ . \quad (2)$$

This compact matrix format not only permits an assessment of the harmonic content of the time series, but also provides a map of the distribution of cosine parameters associated with the signal (i.e., amplitude, frequency, and phase) as a function of position in the line profile. The significance of these estimates can be gauged by the size of A and by the degree to which the behaviour of adjacent (and nominally independent) wavelengths is similar. Of course, the phase is a completely meaningless quantity unless it is associated with a significant peak at a specific frequency.

In practice, we estimated the properties of the cosine functions associated with the observed variations from the CLEAN components directly, rather than the CDFT (which is generated by convolving the CLEAN components with a Gaussian restoring beam of FWHM of $1/\Delta T$, i.e., the dispersion of the Gaussian is $\sigma_b \approx 0.425/\Delta T$; see Roberts et al. 1987). Frequencies were determined from an amplitude-weighted average of the individual CLEAN components that fell within a restoring beam (i.e., $\pm 3\,\sigma_b$) of the local maximum. The semi-amplitude and phase were determined by summing the real and imaginary parts that fell within the restoring beam when it was centered on the given frequency, and then by applying Eqs. (1) and (2), respectively. This approach has the advantage that accurate values of the cosine parameters can be recovered even when the frequency peak falls between adjacent elements of the frequency grid.

5. The 1995 MEGA campaign

5.1. Period analysis

The CDFTs for the main stellar wind features are illustrated in the four panels of Fig. 5. The central section of each panel shows the power $A^2(\nu_i, \mathrm{V}_{\mathrm{r},j})$ as an image, such that darker shadings indicate larger signals and horizontal bands indicate the presence of the same frequency over an extended range of positions in the line. The upper panels show the distribution of $A^2(\bullet, \mathrm{V}_{\mathrm{r},j})$, i.e., the total amplitude at a given position, which is obtained by summing vertically over all the frequency components $0 \leq \nu \leq \nu_{\max}$ (only a portion of which is illustrated in Fig. 5). Similarly, the right-hand panel shows the horizontal summation of all the columns in the image, $A^2(\nu, \bullet)$, which represents the power summed over the entire line as a function of frequency (i.e., a mean periodogram). The mean spectrum of the time series is plotted in the lower panel to provide a positional reference frame.

Fig. 5 succinctly dissects the variability of these UV wind features. The upper panels show that the power of the fluctuations summed over all temporal frequencies (i.e., the temporal variance) is much larger in the lines than in adjacent pseudo-continuum regions. The variance is concentrated in the absorption trough of the P Cygni profiles, and usually increases toward the terminal velocity. In the case of doublets, both components have similar distributions of power as a function of position, and the differences between lines are largely due to the varying degrees of blending associated with the doublets. Weak variability is detected in the emission lobes of all four lines.

The image portions of Fig. 5 show that during the MEGA Campaign at least three and perhaps as many as five discrete frequencies were responsible for most of the observed temporal variance. These frequencies are indicated by the dark, horizontal bands that slice across most of the absorption trough of the P Cygni profiles, and can sometimes be traced more faintly through the emission lobes. The excellent alignment of the bands from panel to panel shows that the same frequencies are present in all three lines, though the relative amplitudes of the frequencies change from line to line. In decreasing order, the three dominant frequencies are 0.83, 0.41, and 0.07 d^{-1}, which correspond to periods of 1.2, 2.4, and 14.3 days, respectively. The two subsidiary peaks have frequencies of 0.29 and 0.20 d^{-1} (i.e., 3.4 and 5.0 days, respectively).

The significance of the subsidiary peaks is difficult to assess, but they are probably not due to incomplete CLEANing because their offsets from the positions of reliably determined peaks are unrelated to features in the spectral window function. (Artifacts of incomplete CLEANing are visible, particularly for the noisy Si III time series). Fig. 5 shows that the subsidiary peaks occur over a more restricted range of velocities than the dominant peaks and are concentrated near the blue edge of a particular wind feature, which suggests that they might be due to the more complicated, nonsinusoidal variations that occur near v_∞ (as illustrated, e.g., in Fig. 2.).

The interpretation of the 0.07 d^{-1} frequency is also unclear, because the time scale it represents is comparable to the du-

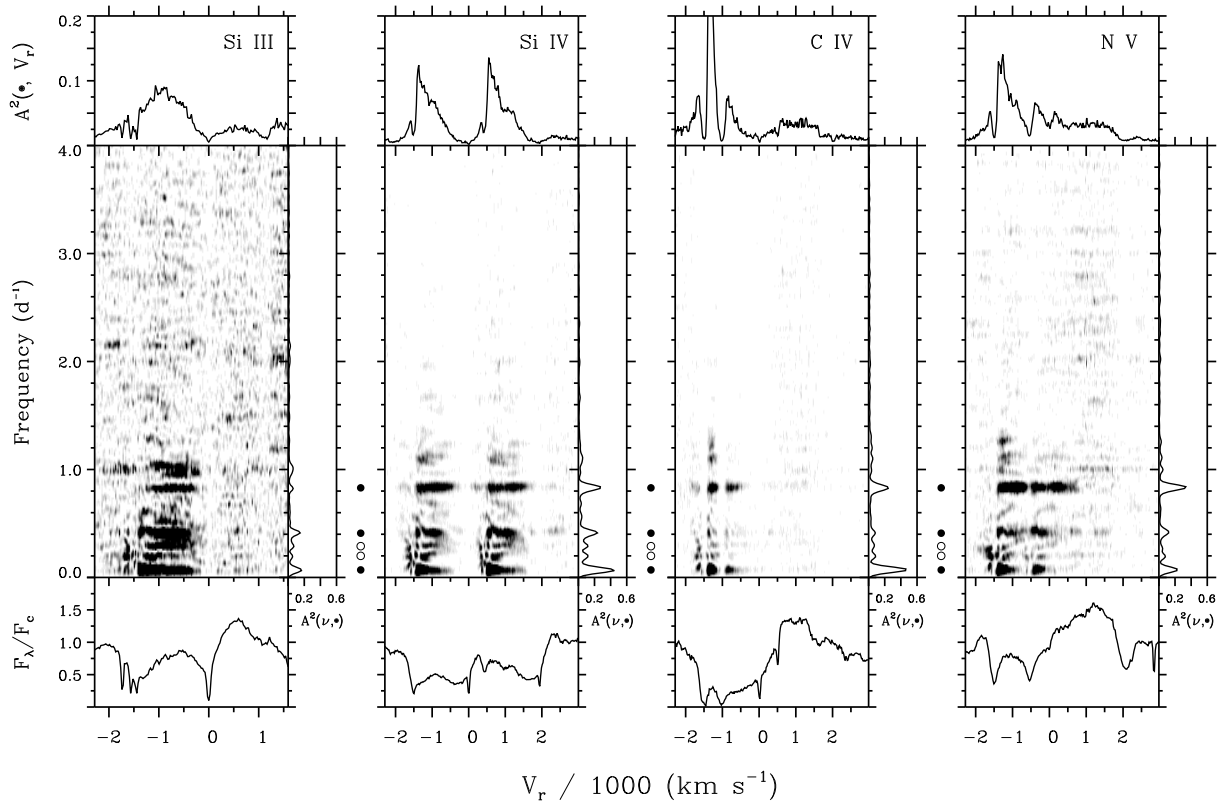

Fig. 5. CDFTs for the MEGA Campaign data of the Si III, Si IV, C IV, and N V resonance lines. Power as a function of position in the line profile and frequency is indicated in the middle panel as an image, in which darker shades denote more power on a linear intensity scale. For each line, the upper panel shows the distribution of power as a function of wavelength, while the right-hand panel shows the distribution of power as a function of frequency. The mean profile from the time series is shown in the bottom panel. Dominant and subsidiary frequencies are indicated by filled and unfilled circles, respectively, placed between the panels.

ration of the MEGA Campaign. The effects of this long-term variation can be seen directly in Figs. 1-3 as the gradual trend for the modulations to occur about a darker flux level with increasing time. However, the cosine properties associated with it are very uncertain, since at most one cycle was observed during the campaign. Despite its large amplitude, we have excluded this long-term variation from the harmonic dissection of the modulations described in the next section.

5.2. Distribution of cosine parameters with projected velocity

The distribution of cosine semi-amplitude, phase, and frequency as a function of position in a P Cygni profile were determined from the CDFTs for the Si III, Si IV, C IV, and N V lines. These are illustrated in Figs. 6 and 7 for the 0.83 d^{-1} ($\equiv$ 1.2 days) and 0.41 d^{-1} ($\equiv$ 2.4 days) frequencies, respectively. For a given line the panels show: the semi-amplitude of the cosine function at each velocity, expressed as a percentage of the continuum; the distribution of the phase constant, ϕ, which runs from $-\pi$ to $+\pi$ and represents the argument of the cosine function at the middle of the time series; and the distribution of the frequency. The mean line profile is plotted in the bottom panel to provide positional reference.

The uncertainties in the various cosine parameters are also indicated in Figs. 6 and 7. In the case of the frequency, one-sigma error bars are shown explicitly. These were determined by the "post-mortem" analysis for power spectra described by Schwarzenberg-Czerny (1991). The uncertainty in the amplitude can be gauged by the noise level in adjacent continuum bands, which is indicated by a dashed line in the top panel and corresponds approximately to 0.5% (Si IV) or 1% (Si III, C IV, N V) of the local pseudo-continuum. These thresholds are significantly lower than the noise level typical of well-exposed *IUE* spectra ($\sim$5%; see Howarth & Smith 1995), since only a single temporal frequency is being considered. Finally, the point-to-point scatter in the phase provides a good indication of the reliability of its determination, because the phase was determined separately for each spectral resolution element, and to good approximation adjacent resolution elements are statistically independent of each other. However, the uncertainty in the phase also depends on the strength of a signal at a particular frequency, and becomes very large when the semi-amplitude is comparable to the background noise level. In order to suppress this scatter, only phases (and frequencies) corresponding to amplitudes greater than the noise level in adjacent continuum bands are included in Figs. 6 and 7.

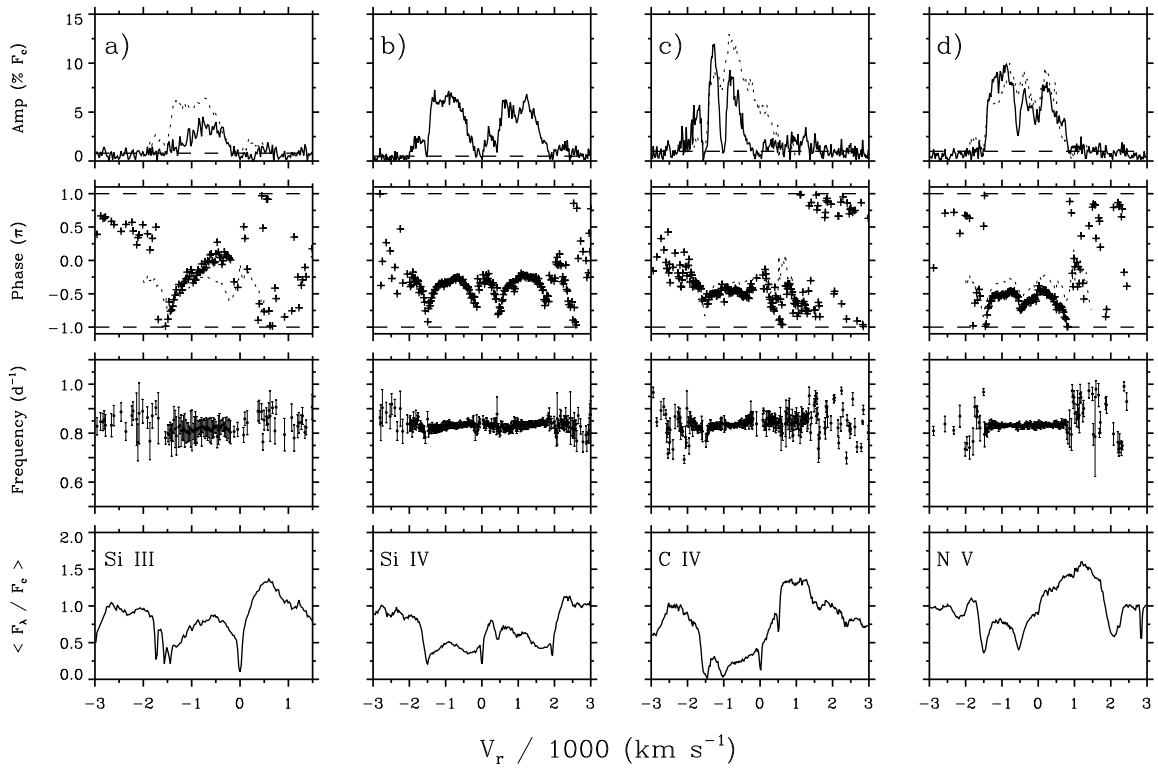

Fig. 6a–d. Distribution of cosine parameters for Si III, Si IV, C IV, and N V for the 1.2-day modulations in the MEGA Campaign data as a function of line-of sight-velocity. From top to bottom, individual panels show the semi-amplitude of the cosine; its phase at the midpoint of the time series; its frequency, and the mean profile. Dashed lines represent reconstructions of the amplitude and phase distributions derived from the unblended components of Si IV.

The Fourier decomposition emphasizes several properties of the modulations that are otherwise difficult to detect in time domain representations. We discuss each of these properties in turn.

5.2.1. A systematic decrease in modulating frequency with V_r?

Fig. 6 suggests that the frequency of the 1.2-day modulations decreases systematically with increasingly negative line-of-sight velocities in the absorption trough of the Si IV doublet, a trend that can also be seen in Fig. 5. A similar, but weaker decrease as a function of position is apparent for the 1.2-day modulations in the C IV doublet, but the effect is evidently not present in the Si III or N V lines. This behaviour was quantified by a weighted linear least-squares fit to the measured frequencies over specified intervals of projected velocity. The results are given in Table 3, together with the weighted mean frequency over the same velocity interval. For Si IV, the slope amounts to a fractional decrease of ∼2.7% of the weighted mean frequency between $V_r = -240$ and $-1480\,\mathrm{km\,s^{-1}}$. Although the mean frequencies agree extremely well for all components and lines, the larger scatter associated with the mean frequency determined from Si IV is an artifact of the presence of the decreasing trend.

Similar trends are not associated with the frequency of the 2.4-day modulations. The weighted mean frequency computed over the specified wavelength intervals (which coincide with those used for the 1.2-day period) are given in Table 4.

Despite the smoothness of the decline of the frequency of 1.2-day modulation in the Si IV doublet and its independent occurrence in both the blue and red components, its significance is not clear. For Si IV, the full range of frequencies over the interval from -240 to -1480 km s^{-1} is only $0.022\,\mathrm{d^{-1}}$, which is comparable to the uncertainty in an individual determination of the frequency at a given position and less than the frequency resolution appropriate to the MEGA Campaign (Table 2). These considerations suggest that the trend may be an artifact of the Fourier analysis. However, the trend is unlikely to be due to the oversampling in frequency used to compute the DFT, since halving or doubling the oversampling factor from its nominal value of 4 did not affect its appearance. The trend is not an artifact of the CLEAN algorithm, since it can also be seen directly in the "dirty" DFT for Si IV. Moreover, if the CLEAN algorithm were somehow responsible, the trend should also be seen in the N V lines, which were analyzed in the same way. Since we cannot at present determine if the trend is spurious, for the remainder of this paper we shall simply assume that the frequency of the 1.2-day modulation is independent of position in a wind profile. From Table 3, the weighted mean frequency of this modulation is $0.832 \pm 0.003\,\mathrm{d^{-1}}$, which corresponds to 1.202 ± 0.004 days.

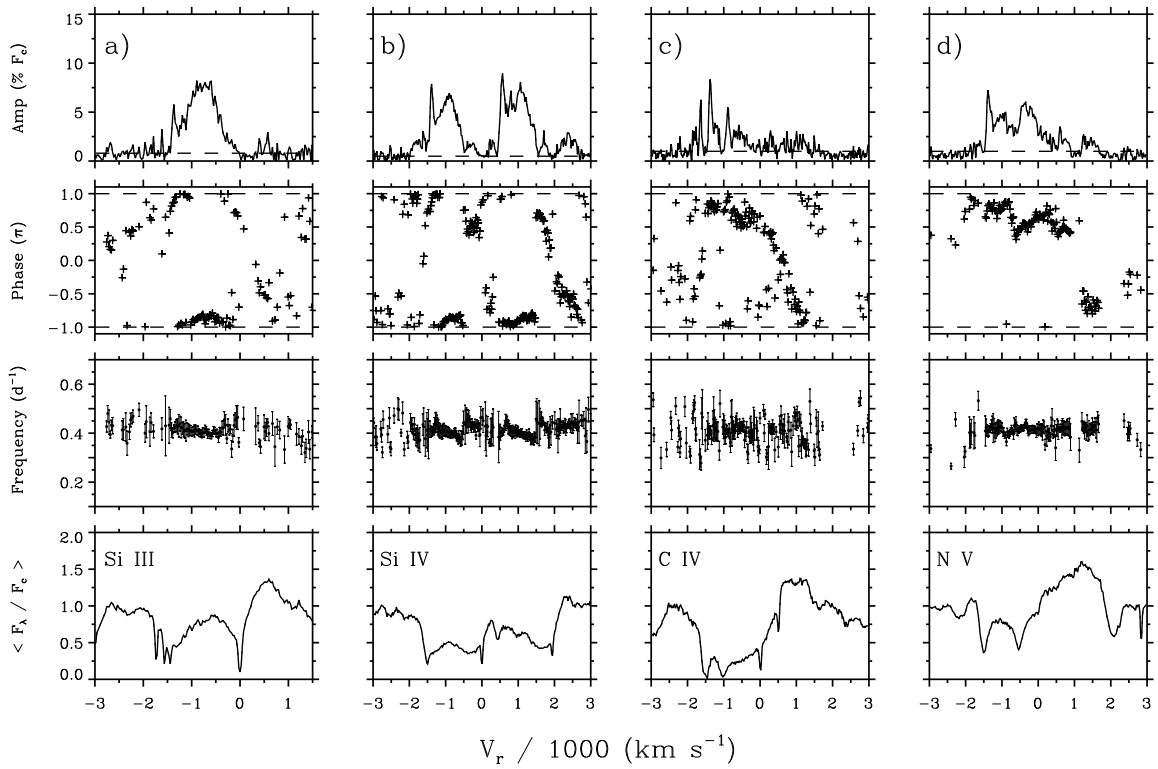

Fig. 7a–d. Same as Fig. 6 but for the 2.4-day period.

5.2.2. Distribution of the phase constant

The most interesting feature of the Fourier decomposition is the systematic distribution of the phase constant as a function of position in the P Cygni profile, particularly in the case of the 1.2-day modulation. Once again, the minimally blended Si IV doublet (Fig. 6) provides a useful entry point for discussing this distribution. The dominant variation is the "convex downward" reversal that extends over most of the width of the absorption trough, and is essentially identical in both components of the doublet. The bending is roughly symmetric about an intermediate line-of-sight velocity, $V_r(\phi_{max}) \approx -710$ km s^{-1}, and encompasses a full range of $\Delta\phi \approx 0.6\,\pi$ radians (see Table 3). This distribution shows that at a fixed time (in this case, the midpoint of the time series), the phase of the 1.2-day modulation is most advanced at approximately -710 km s^{-1}, while the phase of the modulation at positions displaced to either side of this velocity lag by an amount that is roughly proportional to the displacement. Alternately, a fixed phase of the modulation occurs first at $V_r(\phi_{max})$, and only at some later time at larger and smaller velocities. Thus, as previously recognized by Owocki et al. (1995), the "phase bowing" of the 1.2-day period is the Fourier-space manifestation of the tendency for the modulations to bend in the direction of increasing time (Sect. 3). Since the bowing is more plainly evident in Fig. 6 than in the dynamic spectra (Figs. 1 and 3), the Fourier domain appears to be better suited to analyzing this phenomenon quantitatively.

The phase bowing of the 1.2-day modulation is also visible in the N V P Cygni profile (Fig. 6), but is almost completely obliterated in C IV due to the large degree of blending between the components of the doublet. For Si III, the phase distribution in the absorption trough decreases monotonically towards the terminal velocity: i.e., it does not exhibit bowing.

The phase of the 1.2-day modulation shows two other trends as a function of position in the Si IV line: (1) a roughly linear increase in phase at the blue edge of the absorption trough of the blue component of the doublet, between line of sight velocities -1500 and -2000 km s^{-1}; and (2) a linear decrease in phase through the emission lobe of the red component of the doublet, between +2000 and +2700 km s^{-1} on the velocity scale of Fig. 6, which corresponds to a velocity interval of +60 km s^{-1} to +750 km s^{-1} in the frame of the red component. The increase in phase at the blue edge of the blue component (trend 1) is echoed at the blue edge of the red component, but the phase variation through the emission lobe of the red component (trend 2) cannot be traced for the blue component because of blending. These trends are associated with much smaller amplitudes than the modulations of the absorption trough, and can be seen only faintly in the dynamic spectra for Si IV. The increase in phase at the blue edge (trend 1) is also visible in the C IV line, where it exhibits a similar extent in velocity and a positive phase offset with respect to Si IV. Trend 2 might also be present in C IV. However, neither of these trends can be found in the N V line, which does not show any significant amplitude at comparable velocities.

The phase of the 2.4-day modulation also exhibits systematic changes as a function of position in a P Cygni profile (Fig. 7; its measurable properties are listed in Table 4). Phase bowing is again present, though the overall distribution of phase is not as smooth as with the 1.2-day modulation and, in the case of Si IV, "wrapping" (i.e., jumps of $2\,\pi$) makes it harder to see. Much larger phase lags occur with this longer modulation (Table 4). The linear decrease in phase through the emission lobe of the red component of Si IV is better determined, because the amplitude at these velocities is larger. This trend is not particularly evident for the other lines. In contrast to the 1.2-day period, the phase of the 2.4-day modulation decreases sharply at the blue edge of the Si IV line. Again, this trend is not apparent for the other lines.

5.3. Differential phase lags between ions

In order to investigate the extent to which the phase distributions from Si III, C IV, and N V, are consistent with the phase distribution in Si IV, we synthesized them by shifting and coadding template "blue" and "red" amplitude distributions based on the unblended components of the Si IV doublet. The amplitude and phase of the synthesized doublet were determined by fitting a cosinusoidal variation of frequency 0.83 d^{-1} to the coadded signal. The synthesized distributions of these parameters are indicated by dashed lines in the upper panels of Fig. 6.

This approach assumes that the physical structure responsible for the modulations is spatially localized, since it neglects the radiative coupling due to doublet overlap. Comparison of the synthesized and observed amplitude distributions shows that this is a bad assumption in the case of C IV, which is the most severely blended doublet and the most nearly saturated line, but that it is probably acceptable in the case of N V. Although little more can be said about the distribution of cosine parameters in C IV, there do appear to be systematic differences in the distribution of the phase associated with the 1.2-day modulation in Si III and N V with respect to Si IV. In particular, there is a systematic decrease in the value of $\phi_{\max}$ (Table 3; compare also the synthesized and observed distributions of phase in Fig. 6) along the sequence of increasing ionization potential, such that the modulations in Si III *lead* the modulations in Si IV at small velocities in the absorption trough, while the modulations in N V *lag* the modulations in Si IV at all velocities. Thus, it appears that a given phase of the modulation occurs progressively later in lines that diagnose higher energy processes.

The presence of these lags can be shown directly by correlating the modulations at the same line-of-sight velocity in different spectral lines. Fig. 8 compares the correlograms representing the cross-correlation function of Si III with Si IV, the autocorrelation function of Si IV, and the cross-correlation function of N V versus Si IV, all of which were calculated by the method described by Scargle (1989). The time axis in these images has been calibrated in units of the 1.2-day period, so that it represents the phase of the variations directly. The progressive lag as a function of ionization energy is most clearly seen in the dark anticorrelation dip that occurs near a phase lag of 1.5 cycles in the left panel and drifts to a phase lag near 2 cycles in the right panel. The differences between the middle and right-hand panel are small, but consistent with the lag between Si IV and N V indicated in Fig. 6, which amounts to only ∼0.1 cycle.

5.3.1. Distribution of semi-amplitude

The uppermost panels of Figs. 6 and 7 show the distribution of semi-amplitude associated with the 1.2- and 2.4-day modulations, respectively. For the 1.2-day modulations, the semi-amplitude in the unblended line of Si IV is approximately constant at ∼6% of the continuum level over a large fraction of the absorption trough, but eventually falls to the background noise level at $V_r = -1500$ km s^{-1} (i.e., at v_∞) and near $V_r = -160$ km s^{-1}. Smaller amplitude peaks associated with the linear phase trends described in Sect. 5.2.2 can also be seen in the velocity intervals (−2000, −1500) and (0, +450) km s^{-1} (trend 1) and (+2000, +2700) km s^{-1} (trend 2). The semi-amplitude of the 2.4-day modulation is not as uniform, and exhibits a peak near $V_r = -900$ km s^{-1} and a sharper spike at $V_r = -1400$ km s^{-1}. Secondary amplitude peaks are also associated with this modulation at velocities beyond v_∞ and particularly in the interval (+2000, +2500) km s^{-1}, which corresponds to the (unblended) emission lobe of the red component of the doublet. For both periods, the distributions in the blue and red components of the doublet are essentially identical.

As described in the preceding section, the distribution of semi-amplitude in the N V doublet is broadly consistent with the distribution observed in Si IV. In Si III, the semi-amplitude of the 1.2-day modulation is concentrated toward smaller velocities in the absorption trough than Si IV, though this effect is less pronounced in the case of the 2.4-day modulation.

Figs. 6 and 7 also show that there are systematic trends associated with the semi-amplitudes of the 1.2-day and 2.4-day modulations as a function of ionization potential. In particular, the semi-amplitude of the 2.4-day modulation decreases in lines of greater ionization potential, while the semi-amplitude of the 1.2-day modulation shows the opposite behaviour. Thus, the modulations of the low ion Si III are dominated by the 2.4-day period, while the modulations of the high ion N V are dominated by the 1.2-day period. Si IV provides an intermediate case, where the semi-amplitudes associated with both variations are approximately equal.

5.4. Fourier reconstruction of the modulations in Si IV

The information presented graphically in Figs. 6 and 7 permits the periodic component of the wind profile variability to be reconstructed for each velocity as a linear superposition of sinusoidal variations about the time-averaged mean profile:

$$F(V_r, t) = \overline{F} \; + \; \sum_{k=1}^{2} A_k \; \cos\left(2\,\pi\,\nu_k\,[t - \overline{t}] + \phi_k\right) \qquad (3)$$

where $k = 1$ corresponds to the 1.2-day modulation and $k = 2$ corresponds to the 2.4-day modulation, $\overline{t}$ denotes the midpoint of

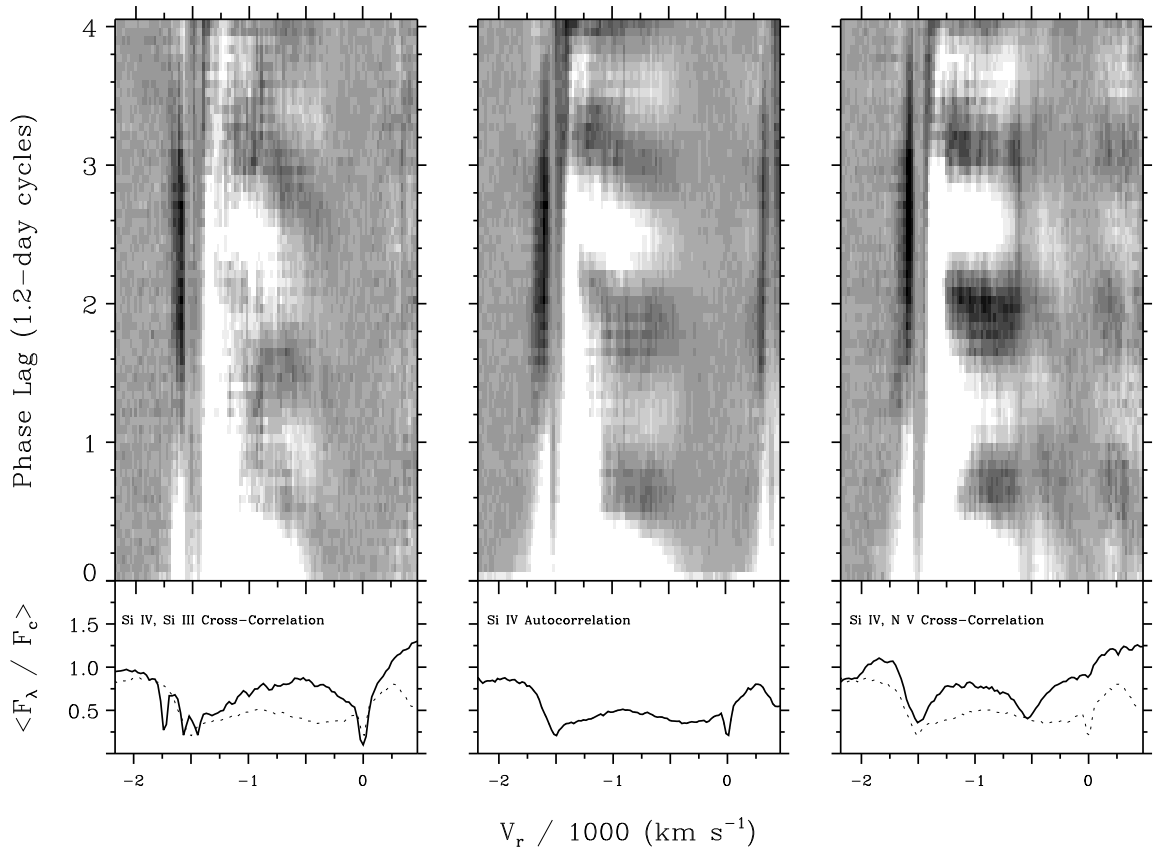

Fig. 8. Correlograms representing the cross-correlation functions of Si III (left) and N V (right) with Si IV, and the autocorrelation function of Si IV (middle). Dark (light) shadings indicate degrees of negative (positive) correlation, and the intensity scale is the same for all images. The mean Si IV profile is shown by a dashed line in the lower panels.

the time series, and $\overline{F}$, A_k, and ϕ_k, (and in principle even ν_k) are all understood to be functions of V_r. Such a Fourier reconstruction is presented for the Si IV doublet in Fig. 9. Since the cosine parameters determined from a Fourier transform are equivalent to those determined by a least-squares fit at prescribed frequencies, this reconstruction may also be viewed as the result of a fit of a two-frequency model to the data.

Fig. 9 has several noteworthy features. First, the dynamic spectrum of residuals shows that the reconstruction based on the 1.2- and 2.4-day periods does not account for all the observed variability, or even for all the variability with these specific periods. These residuals occur because the waveforms are not perfectly sinusoidal (see, e.g., Fig. 2), the long-term trend is not included, and there may be further significant modulation frequencies present in the data (Sect. 5.1). The more interesting residuals are those due to the DACs, which are essentially unaffected by the removal of the modulations. Evidently, these two forms of variability occur independently of each other, i.e., the DACs do not have any significant component of power at temporal frequencies corresponding to 1.2- or 2.4-days. Indeed, the DACs of HD 64760 are not periodic with any period less than $\sim$11 days, which is more than twice the estimated $P_{\rm rot}$.

Second, the phase relationship between the 1.2- and 2.4-day periods is approximately constant, and is such that every second occurrence of the 1.2-day modulation has a slightly larger amplitude. This odd/even effect can also be seen in Fig. 2.

Third, the upward bending of the modulations at large and small velocities due to the phenomenon of phase bowing is more clearly visible in the reconstructed spectra than in the original, noisy data. The faint, linear extensions of the modulations through the emission lobes of the doublet are also more evident, particularly for the red component of the doublet. These redward extensions are more prominent for every second occurrence of the modulation, i.e., they are dominated by the 2.4-day period, as expected on the basis of the semi-amplitudes shown in Figs. 6 and 7. They appear to be continuous with the bending of the modulations at small projected velocities in the absorption trough. Linear extensions of the modulations in the direction of increasing time are also visible in the reconstructed image at large, negative velocities in the absorption trough. Both the blueward and redward linear extensions of the modulations are well modelled by the reconstructed spectra, since there is little or no trace of them in the image of residual spectra.

Finally, the reconstruction emphasizes that the modulations are quite broad in time; i.e., they have significant vertical extent

Table 3. Distribution of cosine parameters for the 1.2-day modulation

Species		Frequency			Phase Bowing		
		V_r range [km s^{-1}]	$\overline{\nu}$ [d^{-1}]	$d\nu/dV_r$ [d^{-1} (km s^{-1})$^{-1}$]	V_r (ϕ_{max}) [km s^{-1}]	ϕ_{max} [π]	$\Delta\phi$ [π]
Si III		(−1480, −240)	0.818 (12)	+1.5 (1.7) × 10^{-5}	...	...	...
Si IV	blue	(−1480, −240)	0.831 (7)	+1.8 (5) × 10^{-5}	−700	−0.261	0.659
	red	(−1480, −240)	0.833 (9)	+2.0 (5) × 10^{-5}	−685	−0.257	0.558
C IV	blend	(−1340, −400)	0.833 (4)	+1.2 (7) × 10^{-5}	−675	−0.425	0.226:
N V	blue	(−1340, −400)	0.831 (3)	−0.6 (6) × 10^{-5}	−710	−0.456	0.996
	red	(−1340, −400)	0.833 (4)	+0.2 (6) × 10^{-5}	−780	−0.451	0.305
Mean:			0.832 (3)		−710 (41)		

One sigma uncertainties are enclosed in parentheses and given in units of the last significant figure.
Colons indicate uncertain measurements.

Table 4. Distribution of cosine parameters for the 2.4-day modulation in 1993 and 1995

Species		Frequency			Phase Bowing		
		Year	V_r range [km s^{-1}]	$\overline{\nu}$ [d^{-1}]	V_r (ϕ_{max}) [km s^{-1}]	ϕ_{max} [π]	$\Delta\phi$ [π]
Si III		1993	(−1100, −240)	0.37 (5)	...	...	...
		1995	(−1480, −240)	0.41 (1)	−605	−0.80:	...
Si IV	blue	1993	(−1100, −240)	0.38 (4)	**−605**	−0.38:	...
		1995	(−1480, −240)	0.41 (2)	−605	−0.82	2.18:
	red	1993	(−1100, −240)	0.37 (3)	**−560**	−0.37:	...
		1995	(−1480, −240)	0.40 (2)	−560	−0.80	1.94:
C IV	blend	1993	(−900, −400)	0.35 (2)	...	...	...
		1995	(−1340, −400)	0.42 (2)	−850:	+1.00:	...
N V	blue	1993	(−1200, −500)	0.41 (4)	**−880**	−0.31:	...
		1995	(−1500, −500)	0.41 (1)	−880:	+1.00:	...
	red	1993	(−1200, −500)	0.40 (2)	**−730**	−0.21	...
		1995	(−1500, −500)	0.42 (2)	−730	+0.76:	...
Mean:				0.41 (1)	−725:		

One sigma uncertainties are enclosed in parentheses and given in units of the last significant figure.
Colons indicate uncertain measurements; bold-faced entries denote assumed values.

in the dynamic spectra, which implies that the physical structures responsible for them must be large.

6. Reanalysis of the 1993 campaign data

6.1. Period analysis

The CDFTs for the Si III, Si IV, C IV, and N V resonance doublets of HD 64760 at the time of the 1993 campaign are presented in Fig. 10. Since this run was ~ 2.7 times shorter than the MEGA Campaign, the frequency resolution is correspondingly worse, as can be seen by comparing the widths of periodogram peaks (right-hand panels) in Figs. 5 and 10. As a result, individual frequency peaks cannot be localized as precisely, and the CLEAN algorithm is less effective in removing the structure of the spectral window from the data.

Nevertheless, Fig. 10 shows that the variations in 1993 also have a periodic component that extends over most of the absorption troughs of the strategic wind lines. Two frequencies appear to dominate the fluctuations: these are particularly clearly seen in the case of N V. As before, the lowest frequency is essentially the same as the duration of the run, and is therefore little more than an indication of the presence of periodic or aperiodic fluc-

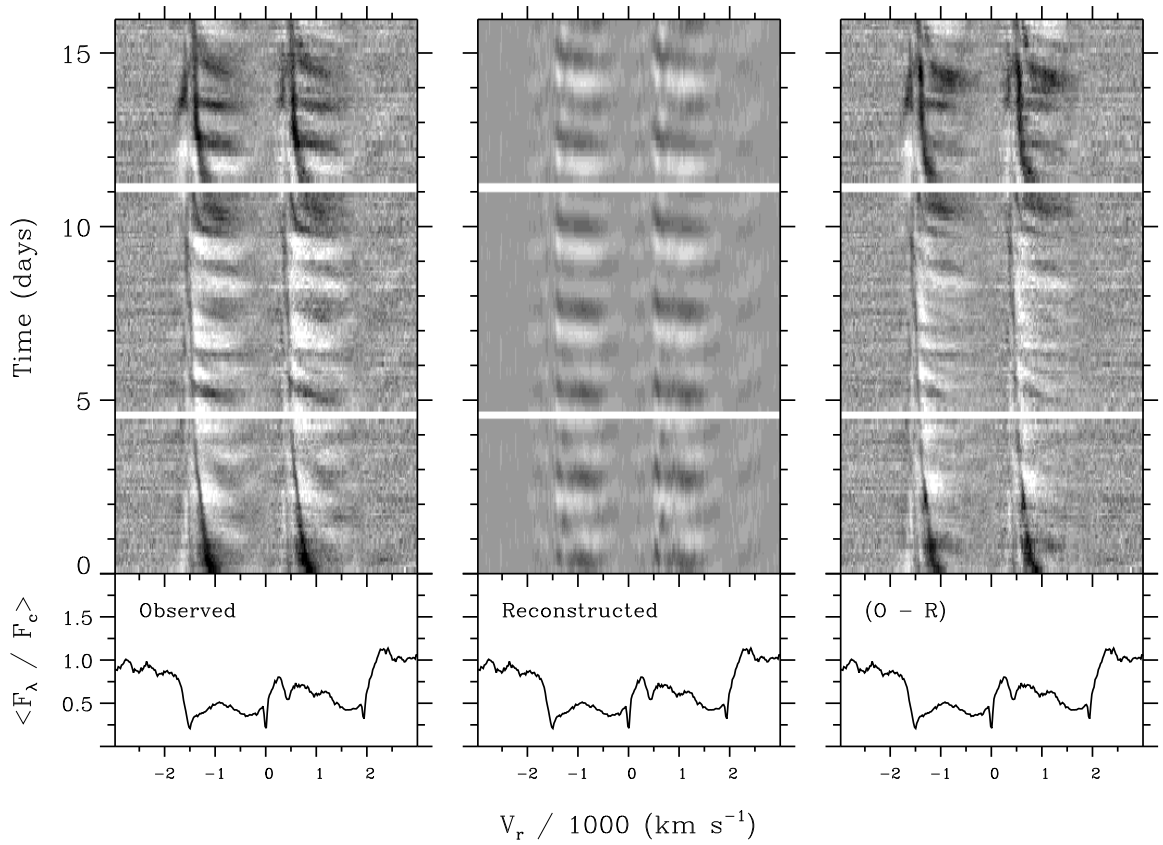

Fig. 9. Fourier reconstruction of the periodic modulations observed in Si IV during the MEGA Campaign. Left: dynamic spectrum of the observed variations, expressed as a difference with respect to the mean spectrum. Middle: dynamic spectrum of the modulations, reconstructed from the cosine parameters for the two frequencies illustrated in Figs. 6 and 7. Right: dynamic spectrum of residuals, in the sense (observed − reconstructed). The grey scale for all images is arranged such that black (white) corresponds to a difference from the mean of −30% (+19%) of the continuum.

tuations on time scales that are longer than 5.8 days. The second period is consistent with 2.4 days, *the same period as observed in 1995*. This can be seen both from the location of the filled circles between the panels in Fig. 10, and from the weighted mean frequencies recorded in Table 4, particularly those for N V. The weighted mean frequency derived from the data from two epochs in Table 4 (excluding the values less than 0.39 d^{-1}, which are unreliable due to confusion with the long-term trend in the 1993 data) is 0.410 ± 0.006 d^{-1}, which corresponds to a period of 2.44 ± 0.04 days. Prinja et al. (1995) also detected this period in equivalent width measurements of the wind lines.

Surprisingly, there is no trace of the 1.2-day modulation that was so dominant in the MEGA data. Since more cycles of it would have been covered in this shorter time series, one might expect that it would be more prevalent than the 2.4-day period. Instead, it appears that the 1.2-day modulation must have had a much lower amplitude in 1993, or have been absent altogether.

6.2. Distribution of cosine parameters with projected velocity

Fig. 11 shows the distribution of cosine parameters associated with the 2.4-day period in 1993 as a function of line-of-sight velocity for Si III, Si IV, C IV, and N V. Since only ∼2.5 cycles of this period were covered, the parameters associated with it cannot be estimated very precisely. This is reflected in Fig. 11 by the size of the error bars on individual frequency estimates, and also in the larger scatter evident in the estimates of the phase constant.

Although it is clear that the distribution of phase with line-of-sight velocity is not random, evidence for phase bowing of the 2.4-day modulation is not as compelling in the 1993 data as in the 1995 data. This is at least partially an artifact of the poorer determination of cosine parameters in the 1993 data. These uncertainties also preclude an accurate determination of the long-term phase coherency of the 2.4-day signal over the 22.5 month (∼280 cycles) between the two observing campaigns.

The distribution of semi-amplitude (top panel in Fig. 11) is also different between the two epochs. In 1993, the semi-amplitude of the 2.4-day modulation was roughly twice as large as the amplitude in 1995 in all lines, and was more strongly concentrated toward lower velocities. The maximum velocity observed at the blue edge of the line was also smaller in 1993; see, e.g., the bottom panel of Fig. 11.

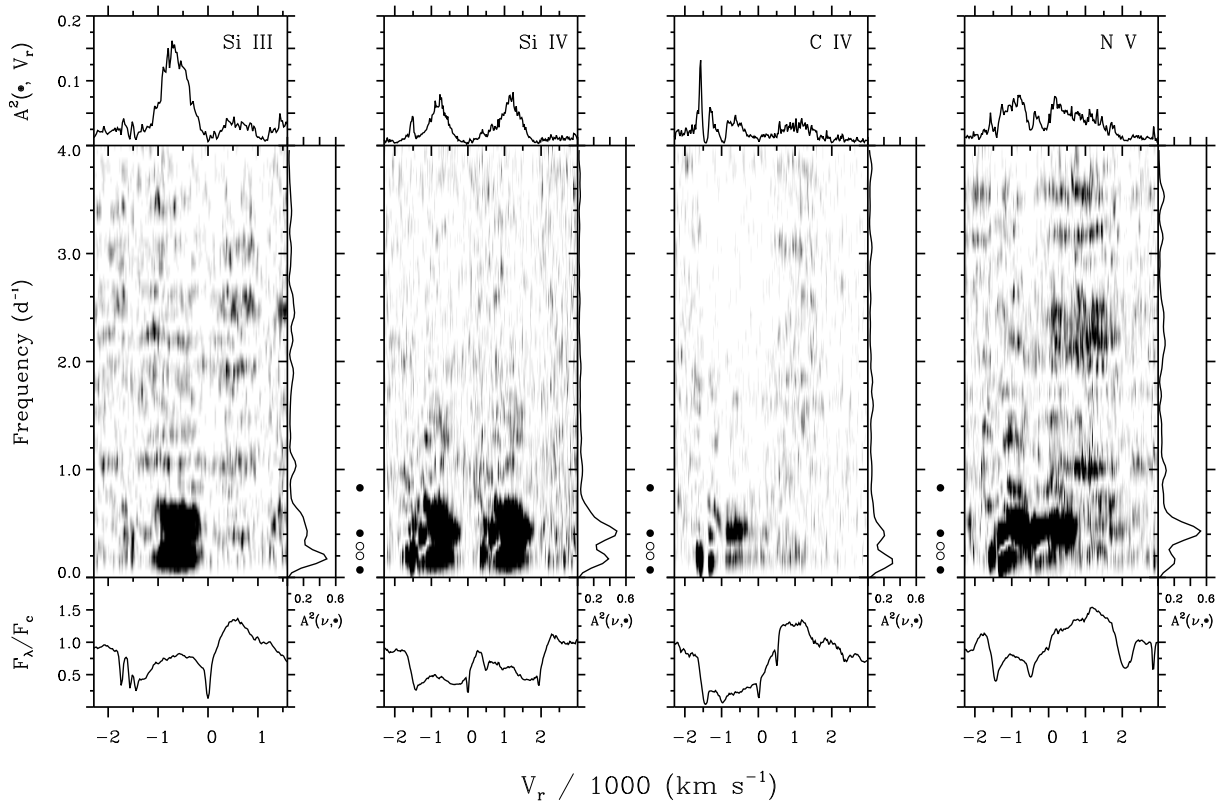

Fig. 10. Same as Fig. 5, but for the shorter time series obtained in 1993. Dominant and subsidiary frequencies from the time of the MEGA Campaign are indicated by filled and unfilled circles, respectively, between the panels. The 2.4-day period was also present in 1993, but the 1.2-day period that dominated the MEGA Campaign data cannot be detected.

7. A model for the modulating wind structures

The dissection of the periodic P Cygni profile modulations by Fourier analysis provides a wealth of diagnostic information about the nature and origin of this new type of stellar wind variability, and serves as the basis for a qualitative model of the wind of HD 64760. This model is based on several inferences from the observations.

7.1. Constraints from time scales

The time series analysis described in the preceding section confirms the detection of periodic variability in the UV wind lines of HD 64760 by Prinja et al. (1995). A 2.4-day period is present in both of the intensive UV data sets available for this star, though most lines in the data from the 1995 MEGA Campaign are dominated by a signal with half this period, 1.2 days. The periodic component of the variability can be represented by a single sinusoidal variation (in 1993) or linear superposition of two sinusoidal variations (in 1995) about the mean value. Consequently, the periodic variations must be viewed as modulations, which are quite distinct from the excess absorptions characteristic of DACs.

The periods of the modulations imply that the structures responsible for them must be closely coupled to processes in the stellar photosphere. From the stellar parameters listed in Table 1, a characteristic radial flow time of the wind of HD 64760 is $t_{\rm flow} \equiv R_\star/v_\infty \approx 2.8$ hours. The shortest period associated with the modulations, 1.2 days, is $10\,t_{\rm flow}$, and these modulations last for at least 15.8 days, or $\sim 135\,t_{\rm flow}$. Thus, the periodic structures are not transient features of the wind, but persist for many flow times over a large range of projected velocities. Since radially outflowing wind material is at least partially replenished during each cycle of the modulation, it seems unlikely that these structures are intrinsic to the wind. Instead, the modulations must be maintained by photospheric processes. This conclusion is bolstered by the observation that the dominant periods are approximately integral submultiples of the estimated rotation period, which implies that there are 2 (e.g., in 1993, when the dominant period of the wind modulations was $\sim P_{\rm rot}/2$) or 4 (e.g., in 1995, when the period of the modulations was $\sim P_{\rm rot}/4$) modulating structures girdling the star.

7.2. Geometric constraints

Two pieces of evidence indicate that the wind structures responsible for the observed modulations are not purely radial, but have significant azimuthal extent and are probably spirals.

First, the covariability of the emission lobe in 1995 indicates directly that the structures are extended around the circumfer-

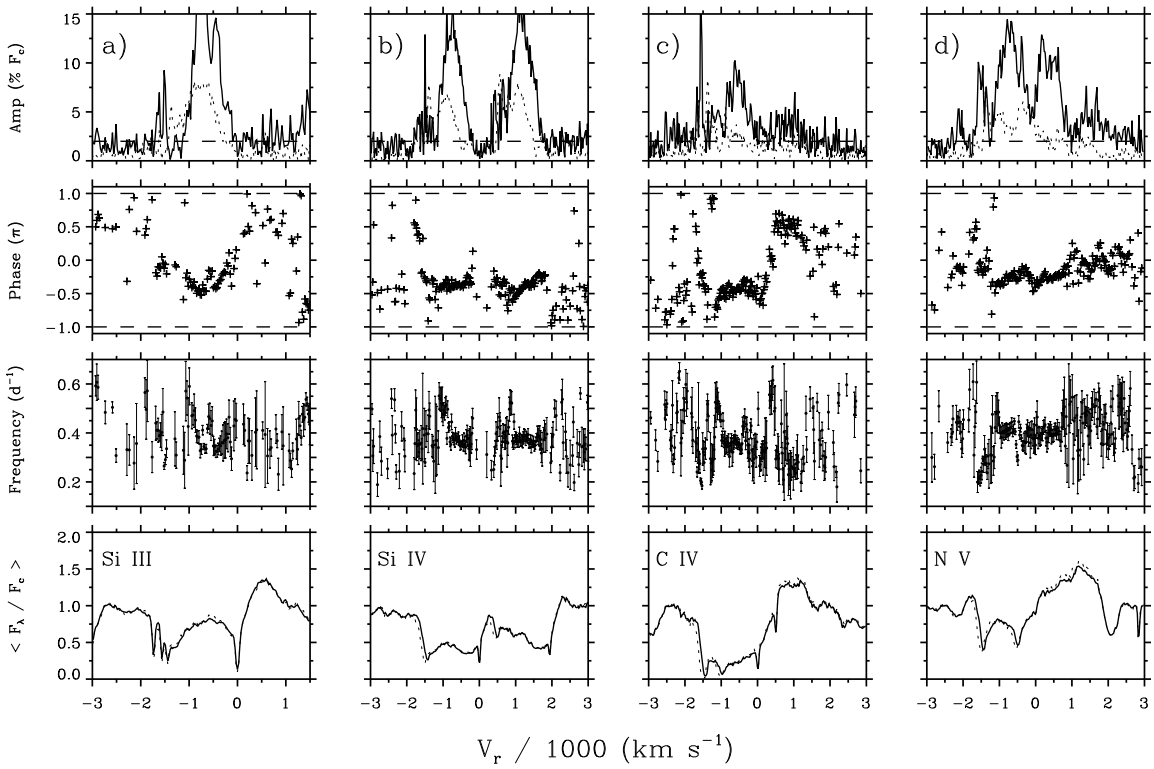

Fig. 11a–d. Same as Fig. 7, but for the 2.4-day modulation in 1993. The semi-amplitudes and mean profiles from the MEGA Campaign are shown as dashed lines.

ence of the star. These variations are smooth extensions in time of the low-velocity portion of the "phase bowing" observed in the absorption trough of Si IV and N V, which implies that the emission variability is due to the same structure when it is not seen projected against the disk of the star. As these variations propagate linearly through the emission lobe, they are accompanied by related variations at large, negative velocities; i.e., the same modulation occurs simultaneously at large, negative velocities in the absorption trough and intermediate, positive velocities in the emission lobe. This is not possible for a structure that is purely radial, but can be accounted for quite naturally by a structure that extends for more than 90° in azimuth.

Second, the phase bowing of the 1.2-day modulation also implies that the wind structures extend over a large azimuthal range (Owocki et al. 1995). The distribution of phase with line-of-sight velocity cannot be understood in terms of a signal that propagates radially outward, since the temporal phase for such a signal is a monotonic function of the line-of-sight velocity. Neither can it be due to a radially extended structure that corotates with the stellar surface, since at any instant such a structure produces a constant phase over a range of projected velocities that is determined by the radial extent of the structure and the radial velocity law governing the expansion of the mean wind.

Instead, phase bowing is a natural consequence of two-dimensional, spiral-shaped structures that corotate (or nearly corotate) with the star. At any instant in time, one of these spiral-shaped structures cuts across a wide range of projected velocities (unlike a radially propagating signal), but exhibits phase lags for different velocities (unlike a purely radial structure) owing to the curvature of the spiral. These lags are determined by the ratio of the azimuthal velocity field (due to rotation) and the radial velocity field (due to the overall expansion of the wind), and the density contrast between the material within the structure and the ambient wind.

This explanation for the origin of phase bowing is illustrated in Fig. 12 (see also Fig. 3 of Owocki et al. 1995), which shows a cross section through the equatorial plane of a stellar wind. Contours of equal line-of-sight velocity for a distant observer looking along the x-axis (dotted lines) are shown for the two-dimensional velocity field described in Sect. 7.5, with v_0 = 18 km s^{-1}, v_∞ = 1500 km s^{-1}, and $v_{\rm rot}$ = 240 km s^{-1}. Spiral-shaped loci show the path followed by material emerging from a fixed longitude on the stellar equator according to this velocity field; consequently, these loci are "streaklines" of the flow. The streaklines are drawn for 10 equally spaced times covering the half rotational cycle when the point of origin is visible to the observer, starting from the entrance to the visible hemisphere (lowermost spiral) and ending with the exit from the visible hemisphere (uppermost spiral). In contrast to an individual fluid parcel (which lags behind the rotating star *along* a given streakline), the streakline corotates (or nearly corotates) with the star and can be used to label a particular temporal phase of the modulations; say, e.g., the phase of maximum flux. Thus, the spirals in Fig. 12 show the evolution of a *fixed phase* of the

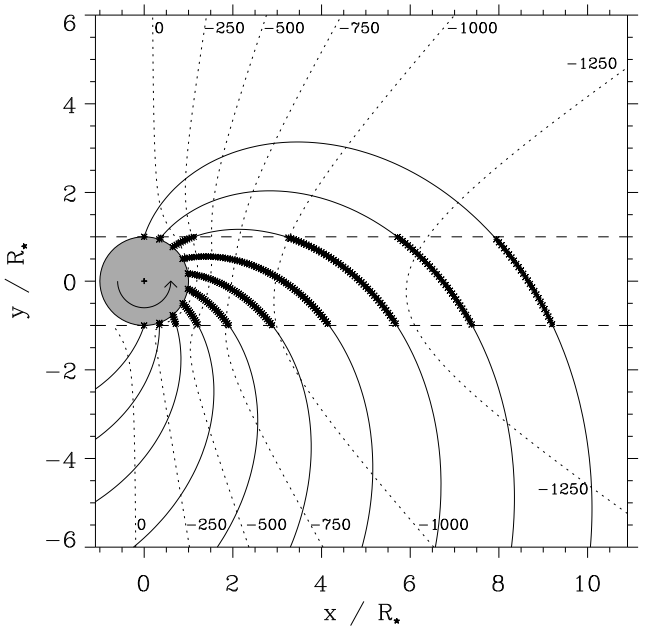

Fig. 12. Cross-section through the equatorial plane of an idealized stellar wind from a rotating star that contains spiral-shaped perturbations. Selected isovelocity contours are shown as dotted lines for the velocity field described in the text, and are labelled by the line-of-sight velocity for a distant observer looking along the x-axis. Spiral streaklines emanating from a fixed stellar longitude are shown for 10 equally spaced times, and segments that fall within the P Cygni absorption trough are highlighted. The spiral first exits the trough near a projected velocity of -750 km s^{-1}, and thereafter exits simultaneously at both larger and smaller velocities. Since a streakline corresponds to a fixed temporal phase of the modulation, the observer sees the same modulation phase simultaneously at two different velocities: i.e., the phase distribution is "bowed".

modulation as a function of space, time, and projected velocity. Of course, each spiral-shaped structure is responsible for a full cycle of the modulation, not just the single phase illustrated, which implies that the spirals are quite broad, on the order of 90° near the stellar surface in the case of the 1.2-day modulations observed during the MEGA Campaign. At any instant the same phase of the preceding (following) spiral arms leads (lags) the arm in the illustration by multiples of 90°.

As the central streakline moves into the hemisphere facing the observer it extends over a progressively greater range of radii in the column of wind material projected against the stellar disk, and so it influences a successively wider range of line-of-sight velocities in the absorption trough of an unsaturated P Cygni profile. However, when the streakline *exits* the absorbing column, its modulating influence is first lost at an intermediate velocity, which is defined by the position at which the spiral is tangent to the edge of the absorption column on the receding side of the rotating star. Thereafter, the streakline exits the absorption column simultaneously at both larger and smaller line-of-sight velocities, but only after lingering for some further time. This lingering manifests itself in the time domain as the upward bowing in dynamic spectra (see, e.g., Fig. 1, 3, and 4), which extends linearly into the emission lobe as the near-star portion of the spiral moves to progressively larger velocities in the hemisphere facing away from the observer. In the frequency domain (e.g., Figs. 6 and 7), it is responsible for observed phase reversal about V_r (ϕ_{max}), which is now seen to correspond to the projected velocity at which the spiral first exits from the absorption column.

This interpretation for the phenomenon of phase bowing appears to be quite robust, which implies that phase bowing is a direct, qualitative indicator for the presence of large-scale, azimuthally extended structure. The detailed distribution of phase as a function of position in the absorption trough provides a quantitative, new probe of these structures: see, e.g., Sect. 7.5 for first steps in this direction.

7.3. Structural constraints on the spiral features from differential phase lags between ions

Both the amplitude and the phase of the 1.2- and 2.4-day modulations exhibit systematic trends with ionization potential in the data from the MEGA Campaign. The 2.4-day modulation dominates the variability of low-ionization lines like Si III, while the 1.2-day modulation dominates in high-ionization lines like N V. The origin of this behaviour is not clear, but it suggests that there are differential ionization or density gradients associated with the modulating structures.

Further constraints come from the phenomenon of phase bowing. With the notable exception of Si III, all the major wind lines exhibited phase bowing during the MEGA Campaign. Since $V_r(\phi_{max})$ is essentially the same for all lines (Table 3), the shape of the spiral features responsible for the phase bowing must also be the same, at least to first order (see Sect. 7.5). However, the fiducial value of the phase constant is systematically more negative for N V (and possibly also for C IV) with respect to the value observed for Si IV (Sect. 5.2.2; Table 3). On the other hand, even though it does not show pronounced bowing in the low-velocity part of the absorption trough, the phase constant associated with the variations in the Si III line are systematically less negative than the values observed in Si IV. These small phase shifts can be observed directly in cross-correlation functions (Fig. 8).

In view of the quite different processes that are globally responsible for the formation of these lines – in particular, N V is a "superion" – these subtle differences are likely due to a localized phenomenon; otherwise, the overall appearance of the modulations would also be affected. In terms of the geometric interpretation given above, the lag of N V with respect to Si IV implies that the structures responsible for the modulations of N V exit from the absorption column after the structures responsible for the modulations of Si IV. Conversely, the modulations observed in Si III ions tend to exit from the absorption column earlier than the modulations in Si IV. Consequently, these differential phase shifts suggest that there is an ionization gradient across the broad spiral features, such that low ionization species are found preferentially along the leading sections of the spi-

ral, while more highly ionized species are more prevalent in the trailing sections.

The presence of this gradient provides an additional constraint on the hydrodynamical phenomenon responsible for the maintenance of the spiral-shaped perturbations in the wind. The origin of the gradient is not immediately clear, since the ionization balance in a stellar wind depends in a complicated way on the local density, electron temperature, and radiation field, all of which are interrelated and poorly understood for B-star winds. For example, if the ionization gradient traces only the local density, we would conclude that the leading edge of the spiral is more dense than the trailing edge, since high density favours recombination and the formation of Si III and Si IV, while low density enhances the survival prospects for N V. On the other hand, the presence of the superion N V in the stellar winds of OB stars is usually taken to be a signature of shocks (see, e.g., Pauldrach et al. 1994), and it is possible that this ion traces a shock front along the trailing edge of the spiral through which material flows and cools. Indeed, this is the expected morphology associated with corotating interaction regions (CIRs), which are long-lived, spiral-shaped perturbations in stellar winds that result from longitudinal variations in the boundary conditions that govern the emergence of the wind (Mullan 1984, 1986). In particular, a high-speed wind emerging from one sector interacts with the slow wind that has previously been expelled from an adjacent region to produce a shock along the inner, trailing edge of the spiral perturbation; see, e.g., the hydrodynamic simulations of Cranmer & Owocki (1996).

7.4. Constraints on optical depth variations

In principle, the amplitude of the modulations in the absorption trough of P Cygni profiles provides a diagnostic of the optical depth variations caused by the spiral-shaped structures in the wind, which in turn carries information about the density and velocity gradients associated with the structures. Unfortunately, this information cannot be extracted in a simple, model-independent way, particularly if the wind is not spherically symmetric. Without detailed modelling, there is no way to constrain these properties of the circumstellar wind structures.

Instead, we note that the equality of the semi-amplitude associated with the modulations in both components of, e.g., the Si IV doublet, implies that the structures responsible for the modulations are optically thick. Otherwise, we would expect the usual 2:1 ratio between the strength of the blue and red component to be preserved for the modulations. Of course, the inferred optical thickness does not necessarily imply that there is a great deal of material contained in the structures, since a locally flat velocity gradient will also produce large optical depths.

Since the modulations are optically thick in Si IV, the ratio of the minimum and maximum flux at a given position in the absorption trough indicates the fraction of the visible hemisphere of the star that is not occulted by the structures in the wind. The "covering factor" associated with the structures can be estimated from the data presented in Fig. 6 for the 1.2-day modulation. If the changes in the forward-scattered emission are negligible, then minimum and maximum fluxes are equal to $F_{\rm min} = \overline{F} - A_1$ and $F_{\rm max} = \overline{F} + A_1$, respectively, where the notation of Eq. (3) has been retained. The mean value of $F_{\rm min}/F_{\rm max}$ is 0.75 ± 0.03 over the interval between -1400 and $-600\,{\rm km\,s^{-1}}$ in the blue component of the Si IV doublet, which implies that the covering factor is $\sim$25%. Consequently, if the structures are centered in the equatorial plane, they subtend a polar opening angle of $\sim 30^\circ$.

7.5. $V_r(\phi_{\rm max})$ *as a kinematic diagnostic*

The distribution of phase as a function of projected velocity contains information about the bending of the spiral features, which in turn depends on both the ratio of the azimuthal velocity field to the radial velocity field and the density contrast exhibited by material in and between the spiral arms. As discussed in the preceding section, it is difficult to obtain a model-independent estimate of density contrast. Moreover, considerable phase mixing occurs at small projected velocities in the absorption trough, because a large range of surface longitudes contribute to the flux at these low velocities. Thus, detailed hydrodynamical modelling and spectral synthesis is required to extract all the information encoded in the shape of the phase distribution.

For the time being, we content ourselves with illustrating the diagnostic potential of the phase distribution by interpreting $V_r(\phi_{\rm max})$ in terms of a kinematical model for the spiral streaklines, in which the hydrodynamical feedback between density and velocity is neglected. For this model, the degree of bending of a streakline depends only on the azimuthal and radial velocity fields of the wind, with the result that streaklines like those shown in Fig. 12 also represent the semi-permanent wind structures responsible for the observed modulations. The shape of a streakline in the equatorial plane is defined by the relation (see, e.g., Cranmer & Owocki 1996)

$$r\,\frac{{\rm d}\phi}{{\rm d}r} = \frac{v_\phi\,(r) - r\,\Omega}{v_r(r; v_0, v_\infty, \beta)} \tag{4}$$

where ϕ is the angle in Fig. 12 between the x-axis and a radial vector measured in the counterclockwise direction, Ω is the angular rotational velocity, $v_\phi(r) = v_{\rm rot}/r$ is the azimuthal velocity, $v_r(r; v_0, v_\infty, \beta) = v_0 + (v_\infty - v_0)\,(1 - 1/r)^\beta$ is the usual "beta-velocity law" governing the wind expansion, and where all spatial variables are expressed in units of the stellar radius. Eq. (4) can be integrated directly to yield the equation of the spiral streakline

$$\phi\,(r) = \phi_0 - \frac{v_{\rm rot}}{v_\infty}\,I(r; w_0, \beta)\ , \tag{5}$$

where $\phi_0 = \phi(r = 1)$ and I is the integral

$$I(r; w_0, \beta) = \int_1^r \frac{1 - (1/r)^2}{w_0 + (1 - w_0)\,(1 - 1/r)^\beta}\,{\rm d}r\ , \tag{6}$$

and where the parameter $w_0 = v_0/v_\infty$. The integral cannot be evaluated analytically in general, but can be determined by standard numerical methods. Eqs. (5) and (6) imply that spirals will

be more tightly wound for smaller values of w_0 or v_0, slower radial velocity laws (i.e., larger β), and larger values of $v_{\rm rot}/v_\infty$.

Since the spiral pattern is assumed to corotate with the stellar surface, its position at any time is given by

$$\phi(r,\,t) = \frac{2\pi\,(t-t_0)}{P_{\rm rot}} + \phi_0 - \frac{v_{\rm rot}}{v_\infty}\,I(r;w_0,\beta) \qquad (7)$$

where the constant is now $\phi_0 = \phi(r = 1,\, t = t_0)$. A given radius *exits* the absorption trough at $t = t_e$ when $\phi(r,\,t_e) = \arcsin(1/r)$; hence

$$t_e(r) = t_0 + \frac{P_{\rm rot}}{2\pi}\left(\arcsin(1/r) - \phi_0 + \frac{v_{\rm rot}}{v_\infty}\,I(r;w_0,\beta)\right)\,. \qquad (8)$$

The radius that *first exits* the absorption column, r_1, can be determined by minimizing $t_e(r)$, which leads to an equation for r_1 in terms of the radial velocity law (which enters due to the differentiation of $I(r;w_0,\beta)$) and the rotational velocity:

$$r_1\;\left(v_r\,(r_1)\right)\;-\;v_{\rm rot}\;\left(r_1^2-1\right)^{\frac{3}{2}} = 0\;. \qquad (9)$$

As argued in Sect. 7.2, the line-of-sight velocity at $(r,\phi) = \left(r_1,\,\arcsin\left(1/r_1\right)\right)$ is just the line-of-sight velocity at which the maximum of the phase distribution is observed, $\mathrm{V_r}(\phi_{\rm max})$. Thus, in terms of the components of the radial and azimuthal velocity fields projected onto the observer's line of sight, we have (with the usual astronomical sign convention for velocities):

$$-\mathrm{V_r}(\phi_{\rm max}) = \cos\phi_1\;\left(v_r\,(r_1)\right) - \sin\phi_1\;\frac{v_{\rm rot}}{r}\quad. \qquad (10)$$

After substituting for $v_{\rm rot}$ from Eq. (9), and noting that $\sin\phi_1 = 1/r_1$, $\cos\phi_1 = (r_1^2-1)^{\frac{1}{2}}/r_1$, there results

$$r_1\;\left(v_r\,(r_1)\right)\;\left(r_1^2-2\right) + \mathrm{V_r}(\phi_{\rm max})\;\left(r_1^2-1\right)^{\frac{3}{2}} = 0\;, \qquad (11)$$

which can be solved by standard numerical methods for assumed values of v_0 and β and measured values of $\mathrm{V_r}(\phi_{\rm max})$ and v_∞. Substitution of the value of r_1 so determined into Eq. (9) yields an estimate of $v_{\rm rot}$ that is independent of direct spectroscopic measurements.

This simple kinematic model was applied to HD 64760 by using the observed value of v_∞ (Table 1) and $\mathrm{V_r}(\phi_{\rm max})$ (Table 3; Si IV values), and solving Eq. (11) for a range of assumed values of β. A fixed value of $v_0 = 15$ km s^{-1} was assumed in all cases, since the shape of the spiral structure is not very sensitive to small changes in the value of this parameter. The results are given in Table 5, where successive columns list the assumed value of β, the derived radius of first exit, and the inferred value of $v_{\rm rot}$. Since an inclination of 90° was explicitly assumed in Eqs. (4) to (11), we can compare the deduced value of $v_{\rm rot}$ directly with the measured value of $v\sin i$ (Table 1) to constrain the spatial gradient of the radial velocity law. For example, Table 5 shows that "fast" velocity laws characterized by $\beta \lesssim 0.67$ can be ruled out, because rotational velocities in excess of the critical velocity are required to produce the observed bending. Similarly, values of $\beta \gtrsim 1$ are eliminated from consideration because these "slow" radial expansions require only modest rotational velocities to reproduce a given degree of spiral bending, and the implied rotational velocities are incompatible with the observed $v\sin i$. The observed $v\sin i$ is reproduced with $\beta = 0.97$, which is a bit slower than the value predicted theoretically from spherically symmetric, steady-state models of O-star winds (see, e.g., Pauldrach et al. 1986: $\beta \approx 0.8$), but falls within the range of values determined semi-empirically for galactic O-stars (see, e.g., Puls et al. 1996: $0.75 \leq \beta \leq 1.15$).

Table 5. Constraints on v_r and $v_{\rm rot}$ from $\mathrm{V_r}(\phi_{\rm max})$

β	$r_1/R_\star$	$v_{\rm rot}$ (km/s)	Remarks
0.5	1.846	504	$v_{\rm rot} > v_{\rm crit}$
0.6	1.915	426	$v_{\rm rot} > v_{\rm crit}$
0.7	1.991	361	
0.8	2.074	308	
0.9	2.163	265	
1.0	2.257	229	
1.2	2.459	175	$v_{\rm rot} < v\sin i$
1.5	2.788	123	$v_{\rm rot} < v\sin i$

On the basis of this kinematic analysis, we conclude that the radial expansion of the wind of HD 64760 is not too different from the outflows derived for spherically symmetrical, steady-state models of the winds of early-type stars. This agreement is surprising, since the very existence of the new diagnostic implies that the stellar wind of HD 64760 is not spherically symmetric, stationary, or homogeneous.

The resolution of this apparent contradiction may lie in the nature of the long-lived, spiral-shaped structures. In models of CIRs (Mullan 1984, 1986; Cranmer & Owocki 1996), the wind flows through spiral-shaped perturbations that result from variations in the surface boundary conditions that govern the emergence of the wind. Although the spiral structures are always present, they are maintained by different material passing through them at different times, as in a standing wave; see also Prinja & Howarth (1988) for a discussion of this possibility. Thus, in the context of the CIR model, it is possible that the radial expansion of the wind may not be strongly affected by the presence of the spirals. Of course, the extent to which the spirals affect the density stratification of the wind, and hence the interpretation of spectroscopic diagnostics, remains an open issue. We envisage that further progress can be made by modelling the entire distribution of phase as a function of projected velocity, not just $\mathrm{V_r}(\phi_{\rm max})$.

8. Discussion

An intriguing picture of the stellar wind and photosphere of HD 64760 emerges from the Fourier analysis of the periodic variability of its UV P Cygni profiles. Instead of a spherically symmetric outflow, its wind consists in part of spiral-shaped perturbations that manifest themselves as modulations of the optical depth structure of the wind about a mean state. The perturbations are azimuthally extended, but probably confined to a

layer $\sim 15^\circ$ above and below the equatorial plane. A kinematic analysis suggests that material flows through these structures. Small phase lags between the modulations in different spectral features may indicate the presence of an ionization or density gradient across the width of the spirals, such that the inner (trailing) edge favours the presence of more highly ionized species. The perturbations appear to corotate with the stellar surface, which implies that they are directly linked to a phenomenon situated in the photosphere that causes the stellar wind to emerge differently from adjacent, equally-spaced longitudinal sectors.

This picture of corotating spirals is qualitatively similar to other models that have been proposed to explain the DACs (e.g.,Underhill & Fahey 1984; Prinja & Howarth 1988; Harmanec 1989, 1991). This is not surprising, since spiral structures are an inevitable consequence of any sort of coupling between the surface of a rotating star and the stellar wind; see, e.g., the discussion of azimuthally extended, spiral-shaped CIRs by Mullan (1984, 1986) and Cranmer & Owocki (1996) that result from longitudinal distributions of velocity, density, or luminosity on the stellar surface. However, these similarities are in some cases superficial. For example, Underhill & Fahey (1984) required ejection from a single point above the stellar surface in order to explain the apparent longevity of a DAC within the absorption trough (as well as the difference between the maximum velocity seen in absorption and the asymptotic velocity achieved by a DAC), whereas the model we propose attempts to explain the continuous, periodic modulations of the absorption trough in terms of spiral wind structures emanating from a large range of adjacent stellar longitudes. The model advocated here is more similar to the one proposed by Prinja & Howarth (1988), with the key difference that we are attempting to explain the behaviour of the modulations, not the DACs.

In the remainder of this section, we discuss several issues arising from this picture of the stellar wind HD 64760 in more detail.

8.1. The nature of the photospheric coupling

Magnetic fields or nonradial pulsations (NRP) are the leading contenders for phenomena that divide the stellar surface into distinct regions that might influence the emergence of a line-driven stellar wind. In either of these cases, variations in the shape of photospheric lines are expected; see, e.g., Bohlender (1994) and Gies (1991, 1996) for illustrations of line profile variations in early-type stars due to magnetic phenomena and NRP. Interestingly, Baade (1984) detected line profile variations in the Si III λ4552 and He I λ6678 lines of HD 64760 in short spectroscopic time series of very high quality. He interpreted these variations in terms of NRP, and suggested that two modes were simultaneously excited: one of high order (large $|m|$), which produced rapid "marching bumps", and one of low order ($|m| \approx 2$), which produced slower changes in the overall symmetry of the profile. Baade estimated periods of $\sim$0.1- and $\sim$0.5-days for the high- and low-order modes, respectively, but these values are very uncertain because of the limited time span of his data. The basic interpretation in terms of NRP is certainly plausible, since HD 64760 is sufficiently luminous to fall within the broad region of the H-R diagram where "strange-mode oscillations" are predicted to occur (Kiriakidis et al. 1993).

In contrast, the study of magnetic fields in early-type stars is hampered by the absence of theoretical predictions concerning their strength and geometry, and by the difficulty of obtaining reliable measurements of field strengths (see, e.g., Bohlender 1994). Owocki (1994) has estimated that magnetic fields that would be undetectable by traditional methods might still be sufficient to influence the dynamics of a line-driven stellar wind, and may therefore play a role in shaping their overall structure. The same lines in which Baade (1984) observed profile variations are also tracers of magnetic fields, which can create patchy surface distributions of Si and He under certain circumstances that could also be detected as line profile variability.

The modulations themselves provide little information concerning the nature of the surface phenomenon, since virtually any longitudinal distribution of density, temperature, or velocity in the photosphere of a rotating star could lead to spiral-shaped wind structures. An indirect constraint comes from the long-term behaviour of the periodic wind modulations, which imply that the photospheric phenomenon governing their production evolves slowly over intervals of $\sim$3 $P_{\rm rot}$, but substantially over intervals of 145 $P_{\rm rot}$; i.e., the surface distribution changed from 2 to 4 equally spaced, longitudinal patches over the 22 months between the 1993 and 1995 observing campaigns. It would be remarkable for a large-scale magnetic field to redistribute itself in this way, since such a rearrangement would apparently require the creation of two new magnetic regions. Presumably, only weak fields could be involved in this rearrangement, since the observational manifestations of strong magnetic fields are known to maintain phase coherence for long periods of time (e.g., σ Ori E: Bolton et al. 1987).

However, it is not immediately evident that NRP could produce such a change, either, though a wider range of testable scenarios are possible. The horizontal velocity of any pulsational mode that is present must be quite small, so that the azimuthal motion seen by an observer in an inertial reference frame is dominated by rotation; otherwise, the period of the modulations at a particular epoch would not approximate an integral submultiple of $P_{\rm rot}$. If this condition holds, the pattern of temperature and velocity variations in the photosphere defined by the pulsations will mimic the effect of "fixed spots" over short periods of time. Over longer intervals, the pattern will change in a complicated manner that depends on which modes are excited and the "beat frequencies" between them. Baade's (1984) preliminary results suggest that several modes of pulsation might be simultaneously excited, though the time scales he quoted are much shorter than the 1.2- and 2.4-day periods associated with the stellar wind modulations. It is clearly important to obtain refined estimates of the periods associated with photospheric line profile variations of HD 64760 in order that a more definitive assessment of their relationship with the periods of the modulations can be made.

8.2. The relationship between the modulations and DACs

A puzzling aspect of the time series analysis is the absence of an obvious link between the periodic modulations and the episodic DACs (Sect. 3; Sect. 5.4). Moreover, in the case of HD 64760, there is no strict relationship between the recurrence of DACs and $P_{\rm rot}$: the recurrence time is at least 11 days (Sect. 3), whereas the fundamental assumption underlying our interpretation of the modulations is that $P_{\rm rot} \approx 4 \times 1.2 \approx 2 \times 2.4 \approx 4.8$ days. As a result, it is difficult to interpret the DACs of this object in terms of CIRs, since a DAC must recur at least once per rotation cycle in the straightforward versions of this model. An interesting possibility suggested to us by Dr. Lex Kaper is that the modulations are direct diagnostics of the density enhancement at the spiral-shaped shock interface between fast and slow streams, while the DACs are attributable to an extended plateau resulting from a "kink discontinuity" that propagates behind the interface (as first suggested by Cranmer & Owocki (1996) on the basis of their hydrodynamical simulations of CIRs). This hypothesis accounts naturally for the geometry and ionization gradient inferred for the modulating structures, but requires some extra factor to explain why kinks of sufficient strength to produce observable DACs do not occur all the time. It predicts that DACs should appear at a fixed phase of the modulation; unfortunately, the phase relationship cannot be determined reliably from the two DACs that were observed during the MEGA Campaign, particularly since the first was already present at the start of the time series. Nevertheless, this hypothesis serves as a useful starting point for further investigations into the origin of DACs and their relationship with the structures responsible for the modulations.

Since the MEGA Campaign was designed to determine how the recurrence of DACs is related to stellar rotation periods, it is both ironic that the DACs of HD 64760 do not seem to be directly tied to $P_{\rm rot}$, and fortunate that a new form of variability that is directly coupled to $P_{\rm rot}$ was detected. In this connection, it is difficult to understand why modulations were not detected in the many previous *IUE* campaigns aimed at O stars, since these objects presumably have photospheric processes that are similar to those that affect the wind of HD 64760 (see, e.g., Fullerton et al. 1996). It may be that spiral-shaped structures are intrinsically more difficult to detect in the stellar winds of O-type stars. The winding of a kinematic spiral is determined by the competition between axial rotation and radial expansion, which is largely determined by the ratio $v_{\rm rot}/v_\infty$ (see, e.g., Eq. [5]). Since O-type stars have systematically larger terminal velocities than early B-type supergiants like HD 64760, this ratio will be smaller and their modulating wind structures more nearly radial. This might explain in part why phase bowing was detected for HD 64760 ($v_{\rm rot}/v_\infty \approx 0.16$) but not in the case of the periodic stellar wind variability of the prototypical O star ζ Puppis (HD 66811; spectral type O4 I(n)f; $v_{\rm rot}/v_\infty \approx 0.08$), which was also observed during the MEGA Campaign (Howarth et al. 1995). Paper I describes several other reasons why B supergiants are better suited to studying stellar wind variability than O stars.

It is also likely that a more basic observational selection effect precluded the discovery of rotational modulation of the stellar winds of hot stars. Before the MEGA campaign, monitoring campaigns generally sought to resolve the flow time scales associated with the stellar winds of O-type stars, which are much shorter than the rotational periods of these objects. Consequently, the campaigns were short, typically of 2-6 days duration (e.g., Kaper et al. 1996). Unless they have large amplitudes, slow variations that occur on time scales close to the length of the observing window are very difficult to detect in such time series, for the obvious reasons of sampling. The modulations stand out clearly in the MEGA data because these data sample several consecutive cycles of the relevant physical time scale, $P_{\rm rot}$, with good temporal resolution. Although it is no longer possible to collect similar UV time series of other interesting objects owing to the demise of the *IUE* Observatory, it would be interesting to reanalyze archival data by using the techniques described here in order to search specifically for analogous modulations in the stellar winds of other early-type stars.

8.3. Final remarks

The detection of periodic, rotationally modulated stellar wind variability in HD 64760 provides a new tool to probe the hydrodynamic structure of the expanding atmosphere of this star. In general terms, these modulations show that the wind is not spherically symmetric, smooth or steady, and it remains to be seen whether they represent comparatively minor fluctuations about a smooth underlying wind, or whether they are a dominant component of the outflow. Evidently, these deviations from the standard model for a hot-star wind are the result of an unidentified, large-scale phenomenon in the photosphere that divides the stellar surface into longitudinal sectors. The nature of this phenomenon and the details of how it affects a line-driven stellar wind must be understood in order to have a complete theory of the photosphere and wind of this star.

These results lead more generally to several new avenues of research into the winds of hot stars. First, it is important to determine the incidence of periodic, rotationally modulated wind variability and phase bowing for a large sample of early-type stars. Although HD 64760 is unusual by virtue of its extreme $v \sin i$, the basic physical ingredients responsible for the stellar wind modulations – photospheric variability and rotation – occur very commonly among OB stars. Consequently, we expect the structures responsible for the modulations to be an important component of the stellar winds of many early-type stars, and a careful survey designed to determine the incidence of this form of variability is certainly in order. Without the services of the stalwart *IUE* observatory, the time sampling requirements of such a study presents major challenges for rapid rotators with fast stellar winds like O- and early-B type stars. Consequently, progress in understanding this phenomenon is likely to come from long-term ground-based surveys of early-type stars with long rotation periods and slower winds (e.g., late-B and early-A

type supergiants), like those initiated by the Heidelberg group (see, e.g., Kaufer et al. 1996a,b).

A second, crucial observational task is to identify the origin of the surface structure that shapes the emergence of the stellar wind. This will also be an observationally intensive process, though several groups are already involved with obtaining and analyzing high-quality spectroscopic time series data of a variety of early-type stars. We are in the midst of a large ground-based observational program designed to determine the properties of the photospheric line profile variations of HD 64760, particularly their periods, in order to constrain the nature of the photospheric process directly.

Finally, important theoretical questions remain concerning, e.g., a detailed dynamical understanding of the coupling of variability in the photosphere to the generation of structure in the stellar wind; the geometry of the circumstellar structures (as constrained by the modulation of the emission lobe); the relationship between the modulations and the DACs; and the influence of large-scale, coherent structures in the stellar wind on the mass-loss rates derived from spectroscopic diagnostics. Quite generally, it is difficult to see how large-scale structures can persist in hot-star winds, given that the winds are dynamically unstable on very short time and length scales due to the action of the potent line-driven instability (e.g., Owocki et al. 1988; Feldmeier 1995). The reconciliation of the puzzle posed by the coexistence of variability on both these scales also merits attention.

Acknowledgements. We wish to thank Drs. Andreas Kaufer, Joachim Puls, Achim Feldmeier, Lex Kaper, and Tom Bolton for their detailed comments on this work. The observational phase of this study was supported by NASA grants NAG5-2137 (to A.W.F.) and NAS5-32782 (to D.L.M.); the analysis phase was supported by grant Pu 117/3-1 to J. Puls from the Deutsche Forschungsgemeinschaft, NASA LTSA grant NAG5-3530 to S.P.O., and NASA contract S-57790-Z to Hughes STX (D.L.M.). The final draft of this paper was prepared while A.W.F. was a visitor at ESO headquarters in Garching, and he is grateful to Drs. Dietrich Baade, Lex Kaper and their colleagues for their support and hospitality. This research has made use of the Simbad database, which is operated at CDS, Strasbourg, France.

References

Baade D., 1984, Photospheric velocity fields of early-type supergiants: A preliminary observational report. In: Proc. of the 25th Liège International Astrophysical Colloquium, Theoretical Problems in Stellar Stability and Oscillations. Université de Liège, Liège), p. 115

Bohlender D.A., 1994, Observations of Magnetic Fields in B Stars. In: Balona L.A., Henrichs H.F., Le Contel J.M. (eds.) Proc. IAU Symp. 162, Pulsation, Rotation, and Mass Loss in Early-Type Stars. Kluwer, Dordrecht, p. 155

Bolton C.T., Fullerton A., Bohlender D., Landstreet J.D., Gies D.R., 1987, High Signal / Noise Spectroscopic Observations of the Magnetic Be Star Sigma Orionis E. In: Slettebak A., Snow T.P. (eds.) Proc. IAU Colloq. 92, Physics of Be Stars. Cambridge Univ. Press, Cambridge, p. 82

Cranmer S.R., Owocki S.P., 1996, ApJ 462, 469

Feldmeier A., 1995, A&A 299, 523

Fullerton A.W., Gies D.R., Bolton C.T., 1996, ApJS 103, 475

Giddings J.R., Rees P.C.T., 1989, SERC Starlink User Note 37

Gies D.R., 1991, Nonradial Pulsations and Line Profile Variability in Early Type Stars. In: Baade D. (ed.) ESO Conference & Workshop Proc. No. 36, Rapid Variability of OB-Stars: Nature and Diagnostic Value. ESO, Garching, p. 229

Gies D.R., 1996, O and B-Star Surface Mapping. In: Strassmeier K.G., Linsky J.L. (eds.) Proc. IAU Symp. 176, Stellar Surface Structure. Kluwer, Dordrecht, p. 121

Gies D.R., Kullavanijaya A., 1988, ApJ 326, 813

Harmanec P., 1989, Bull. Astron.Inst.Czechosl. 40, 201

Harmanec P., 1991, Are Rapid Variations of OB Stars Caused by Circumstellar Gaseous Structures? In: Baade D. (ed.) ESO Conference & Workshop Proc. No. 36, Rapid Variability of OB-Stars: Nature and Diagnostic Value. ESO, Garching, p. 265

Henrichs H.F., Kaper L., Zwarthoed G.A.A., 1988, Rapid Variability in O Star Winds. In: Proc. A Decade of UV Astronomy with the IUE Satellite. ESA SP-281, Vol. 2, p. 145

Henrichs H.F., Kaper L., Nichols J.S., 1994, Wind Variability in O-Type Stars. In: Balona L.A., Henrichs H.F., Le Contel J.M. (eds.) Proc. IAU Symp. 162, Pulsation, Rotation, and Mass Loss in Early-Type Stars. Kluwer, Dordrecht, p. 517

Hiltner W.A., Garrison R.F., Schild R.E., 1969, ApJ 157, 313

Hoffleit D., Jaschek C., 1982, The Bright Star Catalogue, 4th edition. Yale University Observatory, New Haven

Howarth I.D., 1992, Stellar-Wind Variability. In: Drissen L., Leitherer C., Nota A. (eds) Nonisotropic and Variable Outflows from Stars. PASPC 22, 155

Howarth I.D., Smith K.C., 1995, ApJ 439, 431

Howarth I.D., Prinja R.K., Massa D., 1995, ApJ 452, L65

Humphreys R.M., McElroy D.B., 1984, ApJ 284, 565

Kaper L., Henrichs H.F., Nichols J.S., et al., 1996, A&AS 116, 257

Kaufer A., Stahl O., Wolf B., et al., 1996a, A&A 305, 887

Kaufer A., Stahl O., Wolf B., et al., 1996b, A&A 314, 599

Kiriakidis M., Fricke K.J., Glatzel W., 1993, MNRAS 264, 50

Massa D., Fullerton A.W., Nichols J.S., et al., 1995a, ApJ 452, L53

Massa D., Prinja R.K., Fullerton A.W., 1995b, ApJ 452, 842 (Paper I)

Mullan D.J., 1984, ApJ 283, 303

Mullan D.J., 1986, A&A 165, 157

Owocki S.P., 1994, Ap&SS 221, 3

Owocki S.P., Castor J.I., Rybicki G.B., 1988, ApJ 335, 914

Owocki S.P., Cranmer S.R., Fullerton A.W., 1995, ApJ 453, L37

Pauldrach A.W.A., Puls J., Kudritzki R.P., 1986, A&A 164, 86

Pauldrach A.W.A., Kudritzki R.P., Puls J., Butler K., Hunsinger J. 1994, A&A, 283, 525

Prinja R.K., 1988, MNRAS 231, 21P

Prinja R.K., 1992, UV Variability in O Stars. In: Drissen L., Leitherer C., Nota A. (eds) Nonisotropic and Variable Outflows from Stars. PASPC 22, 167

Prinja R.K., Howarth I.D., 1988, MNRAS 233, 123

Prinja R.K., Massa D., Fullerton A.W., 1995, ApJ 452, L61

Prinja R.K., Massa D., Fullerton A.W., Howarth I.D., Pontefract M., 1997, A&A 318, 157 (Paper II)

Puls J., Kudritzki R.-P., Herrero A., et al., 1996, A&A 305, 171

Roberts D.H., Lehár J., Dreher J.W., 1987, AJ 93, 968

Scargle J.D., 1989, ApJ 343, 874

Schaller G., Schaerer D., Meynet G., Maeder A., 1992, A&AS 96, 269

Schwarzenberg-Czerny A., 1991, MNRAS 253, 198

Slettebak A., Collins G.W., Boyce P.B., White N.M., Parkinson T.D., 1975, ApJS 29, 137

Underhill A.B., Fahey R.P., 1984, ApJ 280, 712